NASA Technical Memorandum 82712
AIAA-81-1991

An Improved Prediction Method for Noise Generated by Conventional Profile Coaxial Jets

James R. Stone, Donald E. Groesbeck, and Charles L. Zola
Lewis Research Center
Cleveland, Ohio

Prepared for the
Seventh Aeroacoustics Conference
sponsored by the American Institute of Aeronautics and Astronautics
Palo Alto, California, October 5-7, 1981

NASA

AN IMPROVED PREDICTION METHOD FOR NOISE GENERATED BY CONVENTIONAL PROFILE COAXIAL JETS

James R. Stone,* Donald E. Groesbeck,**
and Charles L. Zola†

National Aeronautics and Space Administration
Lewis Research Center
Cleveland, Ohio 44135

E-994

Abstract

A semi-empirical model for predicting the noise generated by conventional-velocity-profile jets exhausting from coaxial nozzles is presented and compared with small-scale static and simulated flight data. The present method is an updated version of that part of the original NASA Aircraft Noise Prediction (ANOP) Program (1974) relating to coaxial jet noise. That method has been shown to agree reasonably well with model and full-scale experimental data except at high jet velocities in the region near the jet axis. Improvements to the basic circular jet noise prediction have been developed since that time which improve the accuracy, especially at high jet velocity and near the jet axis, and are incorporated into the coaxial jet procedure in this paper. The new procedure is more theoretically based and has also been improved by some empirical adjustments.

Introduction

Accurate noise prediction methods are required in order to predict the environmental impact of airport operations on the surrounding communities, as well as for the realistic design of new aircraft and the development of noise reducing modifications to existing aircraft. The prediction method presented herein is an updated, more theoretically based, version of that part of the original NASA Aircraft Noise Prediction Program[1] pertaining to coaxial nozzles with conventional velocity profiles (e.g., inner-stream velocity greater than outer stream velocity). This paper deals only with the noise generated by the exhaust jets mixing with the surrounding air and does not consider other noises emanating from the engine such as narrow-band shock screech or internally-generated noises.

Although the numerous aspects of the mechanisms of noise generation by coaxial jets are not fully understood, the necessity of predicting jet noise has led to the development of empirical procedures. The NASA interim prediction method for jet noise[1] and several different methods based on extension of the Society of Automotive Engineers (SAE) method for circular jets[2] are in current use. The NASA interim method has already been shown to agree reasonably well with model and full-scale static and flight data[3] for low to moderately-high bypass ratio coaxial jets. This interim method[1] is based on a circular jet method (also in Ref. 1) which is accurate only up to jet velocities of about 520 m/sec; however, that circular jet method has since been improved by incorporating a more theoretically justified formulation of source convection effects.[4] The desirability of further minor improvements in the circular nozzle prediction of static directivity and spectra near the peak noise angle was shown by the comparisons of Gutierrez.[5] It is desirable, therefore, to incorporate the improved convection formulation in the conventional velocity-profile coaxial jet mixing noise prediction procedure, along with the empirical improvements motivated by the comparisons of Ref. 5 and some minor changes in the treatment of flight effects.

For the case of supersonic primary (inner-stream) and/or secondary (outer-stream) jets, broadband shock/turbulence interaction noise must also be considered. The purely empirical shock noise method of Ref. 1 is replaced in the current method by an extensive of the semi-empirical method developed in Ref. 4 for circular jets, which is based largely on the theory of Harper-Bourne and Fisher.[6]

The formulations of these predictions for jet mixing and shock noise are presented in this paper. The validity of these improved predictions is established by fairly extensive comparisons with model-scale static data. Insufficient appropriate simulated-flight data are available in the literature so verification of flight effects must be deferred.

Symbols

(All dimensions are in SI units unless noted.)

A	area
c	speed of sound
D	nozzle hydraulic diameter
F	functional relation (Eq. (4))
F_s	frequency shift parameter defined in Eq. (3)
f	1/3-octave-band center frequency
M	Mach number, V/c
m	exponent defined in Eq. (2)
OASPL	overall sound pressure level, dB re 20 $\mu N/m^2$
p	pressure
R	source-to-observer distance
S	effective Strouhal number
SPL	1/3-octave-band sound pressure level, dB re 20 $\mu N/m^2$
T	total temperature
UOL	predicted OASPL uncorrected for refraction, dB re 20 $\mu N/m^2$
V	velocity
Y	minimum (perpendicular) distance of observer from engine axis (Fig. 1), deg
α	jet angle of attack (Fig. 1), deg
Δ	flight level relative to static, dB
ρ	density

*Head, Section A, Jet Acoustics Branch, AIAA Member.
**Research Engineer, Section A, Jet Acoustics Branch.
†Research Engineer, Mission Analysis Office, AIAA Member.

θ	polar angle from inlet axis (fig. 1), deg
θ'	effective polar angle, $\theta(V_j/c_a)^{0.1}$, deg
θ_M	Mach angle, $180°-\sin^{-1}(1/M_j)$, deg
ϕ	azimuthal angle (Fig. 1), deg
ψ	modified (aircraft) directivity angle (Fig. 1), deg
ω	density exponent (Eq. (A1b))

Subscripts:

a	ambient or apparent
c	convection
D	dynamic
e	effective
F	flight
ISA	international standard atmosphere (288 K and 101.3 kN/m^2)
J	fully-expanded jet
K	kinematic
s	shock noise
90°	parameter evaluated at $\theta = 90°$
0	aircraft
1	fully-expanded primary (inner) jet
2	fully-expanded secondary (outer) jet

Formulation of Procedure

The output of this prediction procedure is an array of SPL spectra at each angle of interest. (Acoustic power relations are not given explicitly, but power computations may be made by integrating the results numerically over all angles.) The procedure calculates the spectra for shock-free jet mixing noise, including the effects of flight. Then, supersonic jet shock noise effects (static and flight) are calculated separately and added antilogarithmically to the shock-free jet mixing spectra. The jet mixing noise and shock noise are assumed to be symmetric about the jet axis. The geometric variables describing the position of the observer relative to the engine are shown schematically in Fig. 1. The noise levels predicted are free-field (no reflections), far-field and lossless (i.e., the effects of atmospheric absorption are not included).

Experimental noise measurements are often made at a distance far enough from the sources to be in the acoustic far-field of each individual source, but not far enough away to treat the entire jet plume as a point source at the center of the nozzle exit plane. When such is the case, comparisons between experimental data and prediction must take source locations into account. The methods used to approximate these source location effects for jet mixing and shock noise are those of Ref. 4, using primary jet conditions. The source position is assumed to be at 4 primary nozzle diameters downstream of the primary exit for a directivity angle, θ, of 0 degrees and to vary linearly with θ to 6 primary diameters at $\theta = 180$ degrees.

Jet Mixing Noise

Olsen and Friedman[7] correlated shock-free cold-flow coaxial jet noise data for secondary-to-primary jet velocity ratios, V_2/V_1, from 0.2 to 1.0 and secondary-to-primary area ratios, A_2/A_1, from 0.67 to 43.5. This correlation was based on extension and modification of the method of Williams, et al.[8]. In the original NASA ANOP interim prediction method for jet noise,[1] the method of Ref. 7 was modified and extended to account for the case of a heated, shock-free primary jet. The approach developed in Ref. 1 and used herein is as follows: (1) the overall sound pressure level, OASPL, and spectra are related to those of the isolated primary jet by means of simple correlation factors; (2) the directivity is taken to be the same as for the isolated primary jet, as indicated by the experimental data of Ref. 7; and (3) the effects of flight are taken to be the same as for the isolated primary jet, as verified in Ref. 3. The prediction methodology is illustrated by a flow chart in Fig. 2. The required inputs are shown at the top of the chart, followed by the logic for calculating the jet mixing noise (single or dual stream) and shock noise (for either one or two streams). The equations, figures and table required at each step are identified. The result is a tabulation of SPL spectra and OASPL as a function of angle.

OOL. - The effects of area ratio, velocity ratio and temperature ratio on the OASPL uncorrected for refraction, OOL, taken from Ref. 1, are shown in Fig. 3, where the OOL relative to that of the isolated primary jet, corrected for temperature ratio,

$$OOL - OOL_1 - 10 \log \sqrt{\frac{T_1}{T_2}}$$

is plotted against an area ratio parameter for various velocity ratios. The temperature ratio term is an empirical approximation. The curves shown correspond to the recommended relation (modified for temperature ratio from Ref. 7),

$$OOL - OOL_1 = 5 \log\left(\frac{T_1}{T_2}\right)$$

$$+ 10 \log\left[\left(1 - \frac{V_2}{V_1}\right)^m + 1.2\,\frac{\left(1 + \frac{A_2 V_2^2}{A_1 V_1^2}\right)^4}{\left(1 + \frac{A_2}{A_1}\right)^3}\right] \qquad (1)$$

In Eq. (1), OOL_1 is the OASPL uncorrected for refraction for the isolated primary jet calculated from the relations given in appendix A, which is based on Ref. 4. The exponent m is given by

$$\left.\begin{aligned} m &= 1.1\sqrt{\frac{A_2}{A_1}};\ \frac{A_2}{A_1} < 29.7 \\ m &= 6.0;\ \frac{A_2}{A_1} \geq 29.7 \end{aligned}\right\} \qquad (2)$$

The ambient temperature data of Ref. 7 are within approximately ±2 dB of the curves shown, with the greatest scatter at a velocity ratio, V_2/V_1, of about 0.6.

Spectra. - The shapes of the sound pressure

level spectra for shock-free coaxial jets were generally found to be similar to those of the isolated primary jet, but with the peak frequency shifted.[7] In Fig. 4 the effect of area ratio and velocity ratio on the frequency shift parameter, F_S, is shown, where

$$F_S = \left(1 - \frac{S_1}{S}\right)\left(\frac{1}{2} + \frac{\frac{T_2V_2A_2}{T_1V_1A_1}}{1 + \frac{T_2V_2A_2}{T_1V_1A_1}}\right)^{-2} \qquad (3)$$

In Eq. (3), S_1 is the effective Strouhal number for the isolated primary nozzle calculated from Appendix A, which is applicable to either a plug or circular core nozzle, and the temperature-dependent term is modified from that used in Ref. 1 to provide proper limiting behavior. The previous formulation[1] did not include the influence of velocity ratio and area ratio on the temperature effect, and it was limited to T_1/T_2 only slightly less than 1.0. From Eq. (3) and Fig. 4, the non-dimensionalized frequency ratio (coaxial to isolated primary), S/S_1, can be calculated, which gives the frequency shift relative to the isolated primary nozzle. The SPL(f) can then be obtained from Table I.

OASPL. - The overall sound pressure level is obtained by integrating the spectral results over the frequency range of interest.

Shock Noise

The shock noise, for each stream which is supersonic, is calculated separately by an extension to the circular jet method developed in Ref. 4. It is assumed that there is no interaction between the two streams. That method was evolved from the model of Harper-Borne and Fisher[6] and the experimental results of Seiner and Norum.[9] The overall sound pressure level uncorrected for refraction, for either stream which is supersonic, $OOL_{s,j}$, is given by

$$OOL_{s,j} = \text{Const} + 10\log\left[\left(\frac{\rho_a}{\rho_{ISA}}\right)^2\left(\frac{c_a}{c_{ISA}}\right)^4\right] + 10\log\left(\frac{A_j}{R^2}\right) + 10\log\left[\frac{\left(M_j^2 - 1\right)^2}{1 + \left(M_j^2 - 1\right)^2}\right] - 10\log[1 - M_o\cos\phi] + F(\theta - \theta_M) \qquad (4)$$

where ϕ is the angle of the observer relative to the direction of aircraft motion, the Mach angle is given by $\theta_M = 180^\circ - \sin^{-1}(1/M_j)$, and the subscript $j = 1$ refers to the primary (inner) stream and $j = 2$ refers to the secondary (outer) stream. The function F is given by

$$F = 0 \quad \text{for} \quad \theta \le \theta_M$$

$$F = -0.75 \quad \text{for} \quad \theta > \theta_M \qquad (4a)$$

The appropriate nondimensional frequency parameter, again based on the Harper-Borne and Fisher[6] model, is given by

$$S_{s,j} = \left(\frac{fD_j}{0.7V_j}\right)\sqrt{M_j^2 - 1}\,(1 - M_o\cos\phi)$$

$$\times\sqrt{\left[1 + 0.7\left(\frac{V_j}{c_a}\right)\cos\phi\right]^2 + 0.0196\left(\frac{V_j}{c_a}\right)^2} \qquad (5)$$

where D_j is the hydraulic diameter. Note that the convection velocity factor is 0.7, instead of the 0.62 value used for jet mixing noise, but the 0.2 value of the turbulent length scale ratio is retained, which leads to the 0.0196 factor. The shock noise peaks at $S_{s,j} = 1.0$ and varies with log $S_{s,j}$ as shown in Fig. 5. The $SPL_{s,j}$ as a function of frequency is then determined from Fig. 5, where $S_{s,j}(f)$ is obtained from Eq. (5). Some effects of jet temperature and directivity angle on spectral shape and level have been observed by von Glahn[10] and others for circular jets, and perhaps such effects are also applicable to coaxial jets, but they are not presently included. Shock noise is not projected to be a factor for future high-bypass engines, since both the jet stream conditions are subsonic at takeoff and landing.

Comparisons with Experimental Data

This section contains limited comparisons of the present prediction method with experimental data for model coaxial jets. Although there exists a great deal of additional experimental data with which comparisons may eventually be made, the present comparisons are considered to be sufficient to demonstrate the validity of the procedure. Comparisons with conical nozzle data are presented in Appendix A to illustrate the validity of the conical nozzle basis for the present method.

Static Jet Mixing Noise

Multiple sideline jet noise measurements were obtained by Goodykoontz, et al.[11] for a series of four coaxial nozzles having secondary to primary area ratios, A_2/A_1, from 1.2 to 3.2 and a common primary nozzle diameter of 10.0 cm. Data were obtained at sideline distances of 1.7, 3.0, 5.0 and 7.0 m. Typical multiple sideline data adjusted to a common sideline distance (3.0 m) and corrected for source position as described under Formulation of Procedure are shown in Fig. 6 for the 1.9 area-ratio coplanar coaxial nozzle. Also shown are predictions from the present method and that of Ref. 1. At low frequencies the greater sideline distances appear to provide more accurate experimental data as evidenced by the relatively smooth spectra and the generally good agreement with the present prediction. Similar results were obtained for the smaller area ratios (not shown) and for the conical nozzle case (shown in Appendix A). This result is consistent with the expectation that the low frequency noise producing region is distributed for several diameters downstream of the jet exit, so that relatively large distances are required to reach the geometric far-field. At high frequencies, there is an apparently anomalous reversal of slope which is worse at large propaga-

tion distances. This accentuation of anomalous behavior at large distances is not unexpected, since at large distances the corrections for atmospheric attenuation are large and nonlinear propagation effects might become important. It is also clear that except for angles near the jet axis, the 5.0-m sideline ($Y/D_1 = 50$) data are of good quality, and it is the experimental data from this array which will be used for the remaining comparisons shown in this section.

In addition to demonstrating the quality of the validation data, this figure shows how the present prediction compares with Ref. 1 at primary high jet velocity. (Differences are smaller as V_1 decreases.) The improvement due to the present method for angles of 125° and less is clear. However, at $\theta > 145°$, the superiority of the new method is clear only at low frequency; further improvements may be needed. The method of Ref. 1 gave excessively high levels at large angles, which gave unrealistically high duration penalties in effective perceived noise level calculations, and that problem has been resolved in the present method.

OASPL. - Sideline directivity patterns for each nozzle configuration are shown in Fig. 7. In each case, the secondary conditions are held essentially constant at $V_2 = 215$ m/sec and $T_2 = 279$ K, and the primary conditions are varied widely. It can be seen that the prediction method is reasonably accurate in predicting the noise directivity for this wide range of inner-stream conditions. It can also be seen, by comparing the results for the various configurations, that the effects of area ratio and of noncoplanar exits are predicted reasonably well. It is also significant that the prediction method produces proper limiting results as the velocity ratio, V_2/V_1, and temperature ratio, T_2/T_1, approach unity. Not only does the present prediction agree with the experimental data in this limiting case, but it agrees better with these data than does the noise predicted (Appendix A) for a single-stream circular nozzle operating at the equivalent mixed-flow conditions (velocity, temperature and mass flow rate). The standard deviation of the prediction method with respect to this data set is 1.8 dB, and the average overprediction is 0.5 dB. Data for the other sideline distances (not shown) show similar agreement.

Spectra. - Spectral comparisons for these same conditions are shown in Figs. 8 to 11, for area ratios of 1.2, 1.4, 1.9 and 3.2, respectively. In each case, spectral comparisons are shown at directivity angles of 45°, 90°, 125° and 145°. Generally the agreement is good except at high frequencies near the jet axis; however, this problem appears to be partially with the experimental data, as discussed earlier in reference to Fig. 6, rather than only with the prediction, but further study of this issue appears justified. There is some tendency to overpredict the low-frequency noise and underpredict the high-frequency noise for the case where the conditions of the two streams approach equality. This problem is not a major one however, since the integrated measure, overall sound pressure level, is reasonably accurate, and this is not a case of interest for real engine cycles.

Shock Noise

While shock noise is not likely to be a significant factor for future high-bypass engines, it should be included for generality and for the predictions of the noise for older, lower bypass engines and possible future supersonic transport engines. Therefore, limited directivity and spectral comparisons with the static experimental results of Ref. 11 at supersonic primary conditions are included.

OASPL. - Sideline directivity patterns are shown in Fig. 12 for coaxial nozzles having area ratios of 1.2, 1.4, 1.9, and 3.2 and a primary nozzle diameter of 10.0 cm. In each case, the secondary conditions are held essentially constant at $V_2 = 216$ m/sec and $T_2 = 278$ K, and the primary conditions are varied. At a fully-expanded primary Mach number $M_1 = 1.4$, two temperatures, $T_1 = 1130$ K (Fig. 12(a)) and 600 K (Fig. 12(b)), were tested, producing primary jet velocities $V_2 = 790$ and 570 m/sec. Results are also shown in Fig. 12(c) for a lower Mach number, $M_1 = 1.15$, at $T_1 = 590$ K and $V_1 = 490$ m/sec. In each case the predicted shock noise is indicated by the dash-dot curve, predicted jet mixing noise by the dashed curve and the total predicted noise by the solid curve. The high Mach number, low temperature conditions have the strongest relative contribution of shock noise; this provides the most significant validation of the shock noise prediction, and the agreement is good. At the low Mach number, there is an overprediction of total noise, especially for the large area ratio, which will be further discussed on a spectral basis in the following section. The comparisons at high Mach number indicate not only that the level of shock noise is predicted reasonably well, but that the mixing noise levels are predicted reasonably well even in the presence of shocks in the flow field. Specifically for the high Mach number, the standard deviation is 1.9 dB and the average overprediction is 0.6 dB, about the same as in the subsonic case.

Spectra. - Spectral comparisons for these same conditions are shown in Figs. 13 and 14, for the 1.2 and 3.2 area ratio nozzles, respectively. At the high Mach number, it appears that the shock noise is predicted reasonably accurately, and comparisons at the intermediate area ratios (not shown) are consistent with these results. For the large area ratio (Fig. 1) the shock noise at low Mach number is overpredicted. This very well could be due to the large mass flow of the secondary impinging on the primary, causing an effectively lower primary pressure ratio and Mach number. Perhaps the most important result of these comparisons is that the jet mixing noise prediction validity is demonstrated to an inner-stream jet velocity of at least 790 m/sec.

Flight Effects

The method presented herein was shown in Ref. 12 to predict the static-to-flight OASPL increments for jet mixing noise to within a standard deviation of 1.5 dB for full-scale flight tests. It would be desirable to show that the present method also agrees reasonably well with

simulated-flight model-scale results; however, no appropriate data are available in the open literature. Verification of flight effects must await the publication of sufficient simulated-flight data, or alternatively, full-scale flight data may provide a better source of validation data.

Concluding Remarks

An improved semi-empirical model for predicting the noise generated by jets exhausting from coaxial nozzles with conventional velocity profiles is presented and compared with small-scale static and simulated-flight data. The prediction of jet mixing noise is based on the extensive experimental study and empirical correlation of Olsen and Friedman (1974) for the effect of the secondary (outer-stream) relative to the isolated primary (inner-stream) jet. The isolated primary prediction used as a base in an improved NASA method for conical nozzles (1980). The effect of a primary nozzle plug is included in the prediction, but is not validated in the present paper. The shock noise for a supersonic primary is assumed to be unaffected by the secondary flow and is calculated from a model based on extension of the method of Harper-Bourne and Fisher (1973). The predictions formulated for both sources cover the full angular range from 0 to 180 degrees. There are no inherent limitations on the range of the prediction methods, and comparisons with static model data are presented for primary jet velocities ranging from 200 to 795 m/sec. These comparisons indicate that the overall sound pressure level is predicted within a standard deviation of 1.8 dB.

Appendix A

Single-Stream Jet Mixing Noise Prediction

Formulation

The coaxial jet noise prediction presented herein uses the noise of the hypothetical isolated primary jet as a building block. This appendix presents these primary jet relationships, which are based on Ref. 4, with minor improvements and with the addition of plug nozzle effect from Ref. 1. The overall sound pressure level, without correction for refraction, OOL_1, is given by

$$OOL_1 = 141 + 10 \log\left[\left(\frac{\rho_a}{\rho_{ISA}}\right)^2\left(\frac{c_a}{c_{ISA}}\right)^4\right] + 10 \log\left(\frac{A_1}{R^2}\right) + 10 \log\left(\frac{\rho_1}{\rho_a}\right)^{\omega} + 10 \log\left(\frac{V_e}{c_a}\right)^{7.5} - 15 \log\left[(1 + M_c \cos\theta)^2 + 0.04 M_c^2\right] - 10 \log[1 - M_0 \cos\psi] + 3 \log\left(\frac{2A_1}{\pi D_1^2} + \frac{1}{2}\right) \quad (A1)$$

Where

$$V_e = V_1[1 - (V_0/V_1)\cos\alpha]^{2/3} \quad (A1a)$$

$$\omega = \frac{3(V_e/c_a)^{3.5}}{0.6 + (V_e/c_a)^{3.5}} - 1 \quad (A1b)$$

$$M_c = 0.62(V_1 - V_0 \cos\alpha)/c_a \quad (A1c)$$

The modified directivity angle, ψ, is angle of the observer relative to the direction of aircraft motion. The angle of attack, α, is the angle of the upstream axis of the jet relative to the direction of aircraft motion. For flyover directly over the observer, $\psi = \theta - \alpha$. Spectral relationships are given in Table I, where SPL - OOL is given at various corrected angles, $\theta' = \theta(V_1/c_a)^{0.1}$ as a function of the logarithm of the effective Strouhal number, S. For the single stream case, $S = S_1$, where

$$S_1 = \frac{f\sqrt{4A_1/\pi}}{V_e}\left(\frac{D_1}{\sqrt{4A_1/\pi}}\right)^{0.4} \times \left(\frac{T_1}{T_a}\right)^{0.4(1 + \cos\theta')} [1 - M_0 \cos\psi] \times \sqrt{\frac{\left[1 + 0.62\left(\frac{V_1 - V_0}{c_a}\right)\cos\theta\right]^2 + 0.01538\left(\frac{V_1 - V_0}{c_a}\right)^2}{\left[1 + 0.62\left(\frac{V_1}{c_a}\right)\cos\theta\right]^2 + 0.01538\left(\frac{V_1}{c_a}\right)^2}} \quad (A2)$$

Table I differs somewhat from that given in Ref. 4, in order to produce a more accurate prediction at the peak noise angle and near the jet axis, based on the comparisons of Gutierrez.[5]

Validation

Since minor improvements have been made with respect to Ref. 4, some of the comparisons shown therein with the data of Tanna, et al.[13] are repeated here using the modified prediction. In addition, single-stream results from the facility providing the data used to validate the coaxial prediction[11] are compared with the single jet prediction.

In Fig. A1 spectral comparisons with the data of Ref. 13 are shown at directivity angles of 57, 86, 116, and 155 degrees for jet velocities from 0.8 to 2.55 times the ambient sonic velocity. The agreement is reasonably good. Further comparisons are made in Fig. A2 with the data from various sideline distances[11] for a coaxial nozzle with flow in the inner stream only. The agreement is quite similar to the coaxial results of Fig. 6. The comparsons show that the conical nozzle static jet noise data from the same facility which provided most of the coaxial data utilized herein is in agreement with the prediction.

References

1. Stone, J. R., "Interim Prediction Method for Jet Noise," NASA TM X-71618, 1974.
2. "Gas Turbine Jet Exhaust Noise Prediction," Society of Automotive Engineers, SAE-ARP-876, Mar. 1978.
3. Stone, J. R., "Prediction of In-Flight Exhaust Noise for Turbojet and Turbofan Engines," Noise Control Engineering, Vol. 10, Jan.-Feb. 1978, pp. 40-46.
4. Stone, J. R., and Montegani, F. J., "An Improved Prediction Method for the Noise Generated in Flight by Circular Jets," NASA TM-81470, 1980.
5. Gutierrez, O. A., "Effect of Facility Variation on the Acoustic Characteristics of Three Single Stream Nozzles," NASA TM-81635, 1980.
6. Harper-Bourne, M., and Fisher, M. J., "The Noise from Shock Waves in Supersonic Jets," Noise Mechanisms, AGARD-CP-131, Advisory Group for Aerospace Research and Development, Paris, 1973, pp. 11-1 to 11-13.
7. Olsen, W. A., and Friedman, R., "Jet Noise from Coaxial Nozzles over a Wide Range of Geometric and Flow Parameters," AIAA Paper 74-43, Jan. 1974.
8. Williams, T. J., Ali, M. R. M. H., and Anderson, J. S., "Noise and Flow Characteristics of Coaxial Jets," Journal of Mechanical Engineering Science, Vol. 11, Apr. 1969, pp. 133-142.
9. Seiner, J. M., and Norum, T. D., "Experiments on Shock Associated Noise of Supersonic Jets," AIAA Paper 79-1526, July 1979.
10. von Glahn U., "New Interpretations of Shock-Associated Noise with and without Screech," NASA TM-81590, 1980.
11. Goodykoontz, J. H., and Stone, J. R., "Experimental Study of Coaxial Nozzle Exhaust Noise," AIAA Paper 79-0631, Mar. 1979.
12. Stone, J. R., "An Improved Method for Predicting the Effects of Flight on Jet Mixing Noise," NASA TM-79155, 1979.
13. Tanna, H. K., Dean, P. D., and Burrin, R. H., "The Generation and Radiation of Supersonic Jet Noise, Vol. III: Turbulent Mixing Noise Data," LG76ER0133-Vol-3, Lockheed-Georgia Co., Marietta, GA, 1976. (AD-A032882, AFAPL-TR-76-65-Vol-3.)

TABLE I. - RECOMMENDED SPECTRA FOR JET MIXING NOISE

Frequency parameter, log S	Corrected directivity angle (referred to inlet), $\theta' = \theta(V_j/c_a)^{0.1}$, degrees										
	0°-110°	120°	130°	140°	150°	160°	170°	180°	190°	200°	250°
	Normalized sound pressure level, SPL - UOL, dB										
-3.6	-85.0	-90.0	-95.0	-100.0	-100.0	-100.0	-100.0	-90.0	-80.0	-70.0	-60.0
-1.8	-40.5	-40.4	-40.4	-40.3	-40.1	-39.5	-37.5	-36.0	-35.0	-34.0	-33.8
-1.7	-38.0	-37.8	-37.4	-37.1	-37.0	-36.4	-33.5	-33.0	-32.5	-32.0	-32.0
-1.6	-35.6	-35.4	-34.4	-33.8	-33.5	-33.3	-30.0	-30.0	-30.0	-30.0	-31.0
-1.5	-33.3	-33.2	-31.4	-30.3	-30.0	-29.5	-27.0	-27.0	-27.5	-28.0	-30.0
-1.4	-30.9	-30.9	-29.5	-26.8	-26.4	-25.5	-24.5	-25.0	-25.5	-26.0	-31.0
-1.3	-28.6	-28.6	-25.7	-23.4	-23.0	-22.8	-22.5	-23.0	-23.5	-24.0	-32.5
-1.2	-26.2	-26.2	-22.9	-19.8	-19.4	-20.0	-20.5	-21.0	-21.5	-22.0	-34.5
-1.1	-24.0	-24.0	-20.1	-16.2	-16.8	-17.5	-18.5	-19.0	-19.5	-20.0	-36.6
-1.0	-21.8	-21.8	-17.3	-13.2	-14.5	-16.2	-16.5	-17.0	-17.5	-18.5	-38.8
-.9	-19.5	-19.5	-14.7	-11.2	-13.1	-14.7	-15.5	-16.0	-17.0	-19.0	-40.1
-.8	-17.5	-17.4	-13.0	-10.2	-11.0	-13.5	-14.5	-15.5	-17.5	-20.0	-42.5
-.7	-15.9	-15.6	-11.5	-9.5	-9.4	-12.6	-14.0	-16.5	-18.5	-21.0	-45.0
-.6	-14.7	-14.0	-9.7	-8.8	-8.3	-12.0	-14.5	-18.0	-20.0	-22.0	-47.5
-.5	-13.7	-12.4	-9.0	-8.1	-7.7	-11.7	-15.8	-20.0	-21.8	-23.5	-50.0
-.4	-12.8	-11.0	-8.9	-8.4	-8.3	-12.6	-17.9	-22.2	-24.1	-25.9	-52.5
-.3	-12.1	-10.2	-9.1	-8.9	-9.8	-14.5	-20.0	-24.4	-26.4	-28.3	-55.0
-.2	-11.6	-9.9	-9.6	-9.8	-11.6	-16.4	-22.1	-26.6	-28.7	-30.7	-57.5
-.1	-11.3	-10.2	-10.8	-11.3	-13.4	-18.3	-24.2	-28.8	-31.0	-33.1	-60.0
.0	-11.1	-10.6	-12.0	-12.9	-15.2	-20.2	-26.3	-31.0	-33.3	-35.5	-62.5
+.1	-11.2	-11.1	-13.3	-14.5	-17.0	-22.1	-28.4	-33.2	-35.6	-37.9	-65.0
.2	-11.3	-11.8	-14.6	-16.1	-18.8	-24.0	-30.5	-35.4	-37.9	-40.3	-67.5
.3	-11.7	-12.7	-15.9	-17.7	-20.6	-25.9	-32.6	-37.6	-40.2	-42.7	-70.0
.4	-12.3	-13.7	-17.2	-19.3	-22.4	-27.8	-34.7	-39.8	-42.5	-45.1	-72.5
.5	-13.0	-14.7	-18.5	-20.9	-24.2	-29.7	-36.8	-42.0	-44.8	-47.5	-75.0
.6	-13.7	-15.8	-19.8	-22.5	-26.0	-31.6	-38.9	-44.2	-47.1	-49.9	-77.5
.7	-14.6	-16.9	-21.1	-24.1	-27.8	-33.5	-41.0	-46.4	-49.4	-52.3	-80.0
.8	-15.6	-18.0	-22.4	-25.7	-29.6	-35.4	-43.1	-48.6	-51.7	-54.7	-82.5
.9	-16.7	-19.2	-23.7	-27.3	-31.4	-37.3	-45.2	-50.8	-54.0	-57.1	-85.0
1.0	-17.8	-20.4	-25.0	-28.9	-33.2	-39.2	-47.3	-53.0	-56.3	-59.5	-87.5
1.1	-18.9	-21.6	-26.3	-30.5	-35.0	-41.1	-49.4	-55.2	-58.6	-61.9	-90.0
1.2	-20.1	-22.8	-27.6	-32.1	-36.8	-43.0	-51.5	-57.4	-60.9	-64.3	-92.5
1.3	-21.3	-24.0	-28.9	-33.7	-38.6	-44.9	-53.6	-59.6	-63.2	-66.7	-95.0
1.4	-22.4	-25.2	-30.2	-35.3	-40.4	-46.8	-55.7	-61.8	-65.5	-69.1	-97.5
1.5	-23.6	-26.4	-31.5	-36.9	-42.2	-48.7	-57.8	-64.0	-67.8	-71.5	-100.0
1.6	-24.8	-27.6	-32.8	-38.5	-44.0	-50.6	-59.9	-65.2	-70.1	-73.9	-102.5
1.7	-26.0	-28.8	-34.1	-40.1	-45.8	-52.5	-62.0	-68.4	-72.4	-76.3	-105.0
1.8	-27.2	-30.0	-35.4	-41.7	-47.6	-54.4	-64.1	-70.6	-74.7	-78.7	-107.5
3.6	-48.8	-51.6	-58.8	-70.5	-80.0	-88.6	-101.9	-110.2	-116.1	-121.9	-152.5
OASPL-UOL	.0	+.1	+.5	+1.1	+.4	-3.2	-5.8	-7.7	-9.0	-10.6	

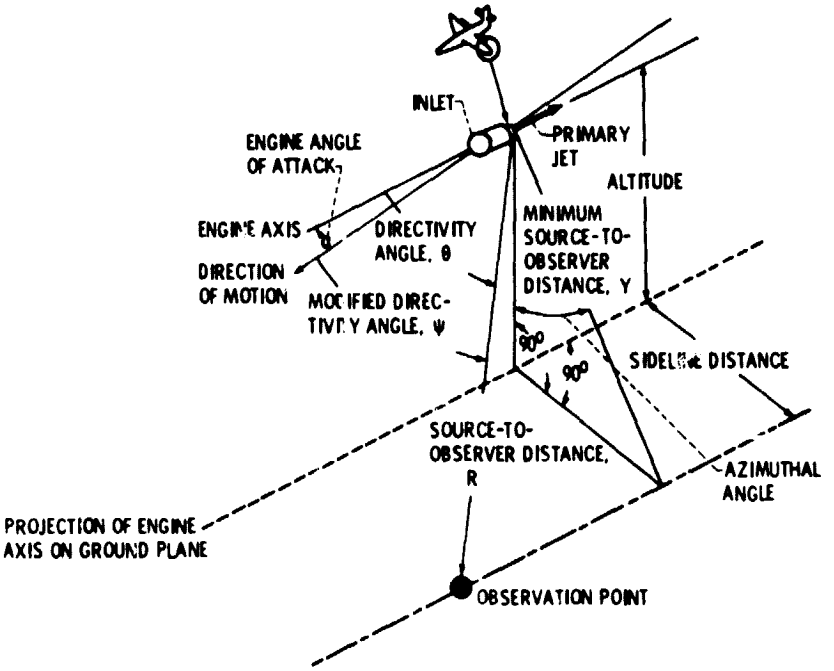

Figure 1. - Geometric variables describing position of airplane noise source with respect to an observation point.

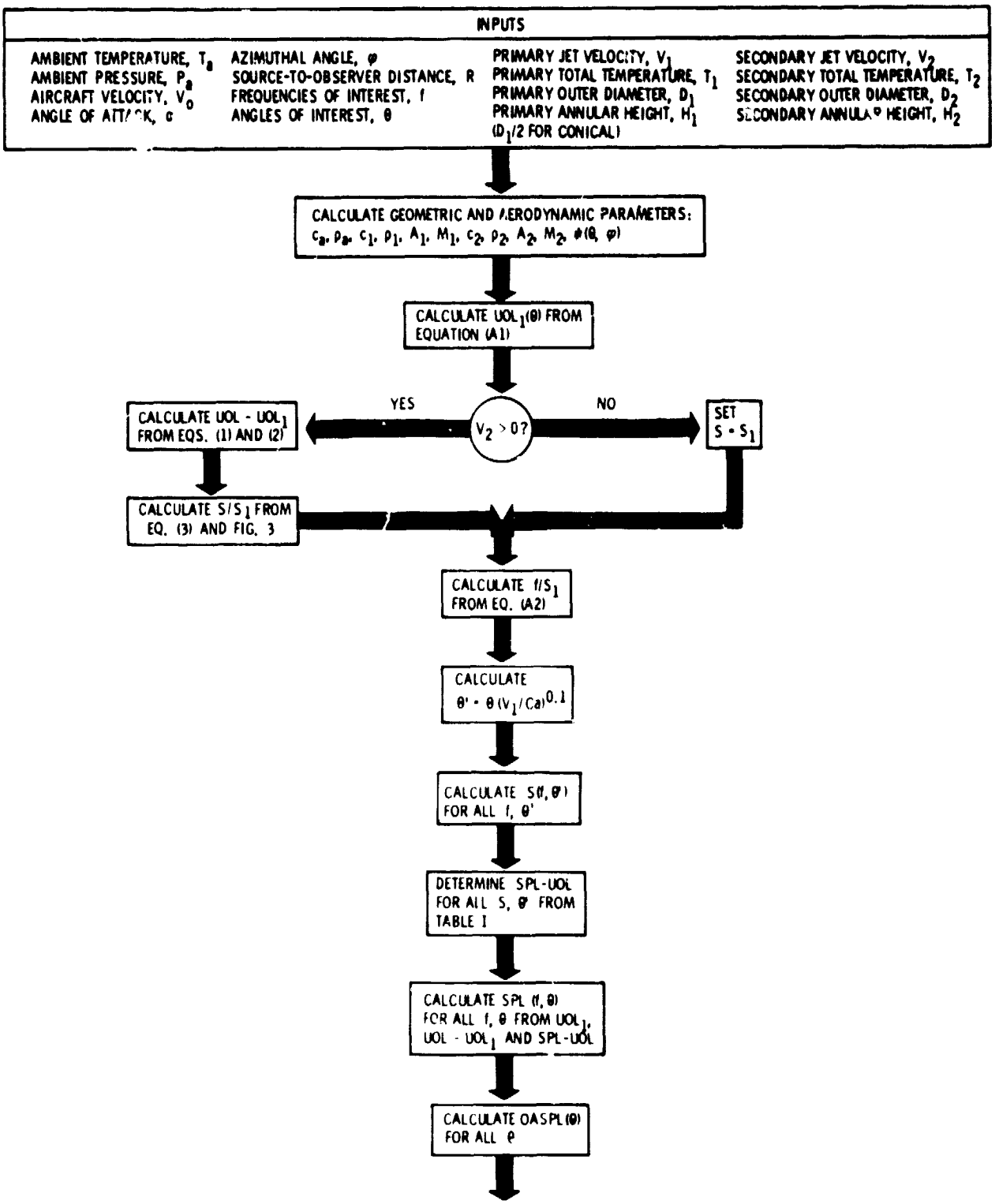

Figure 2. - Prediction flow chart.

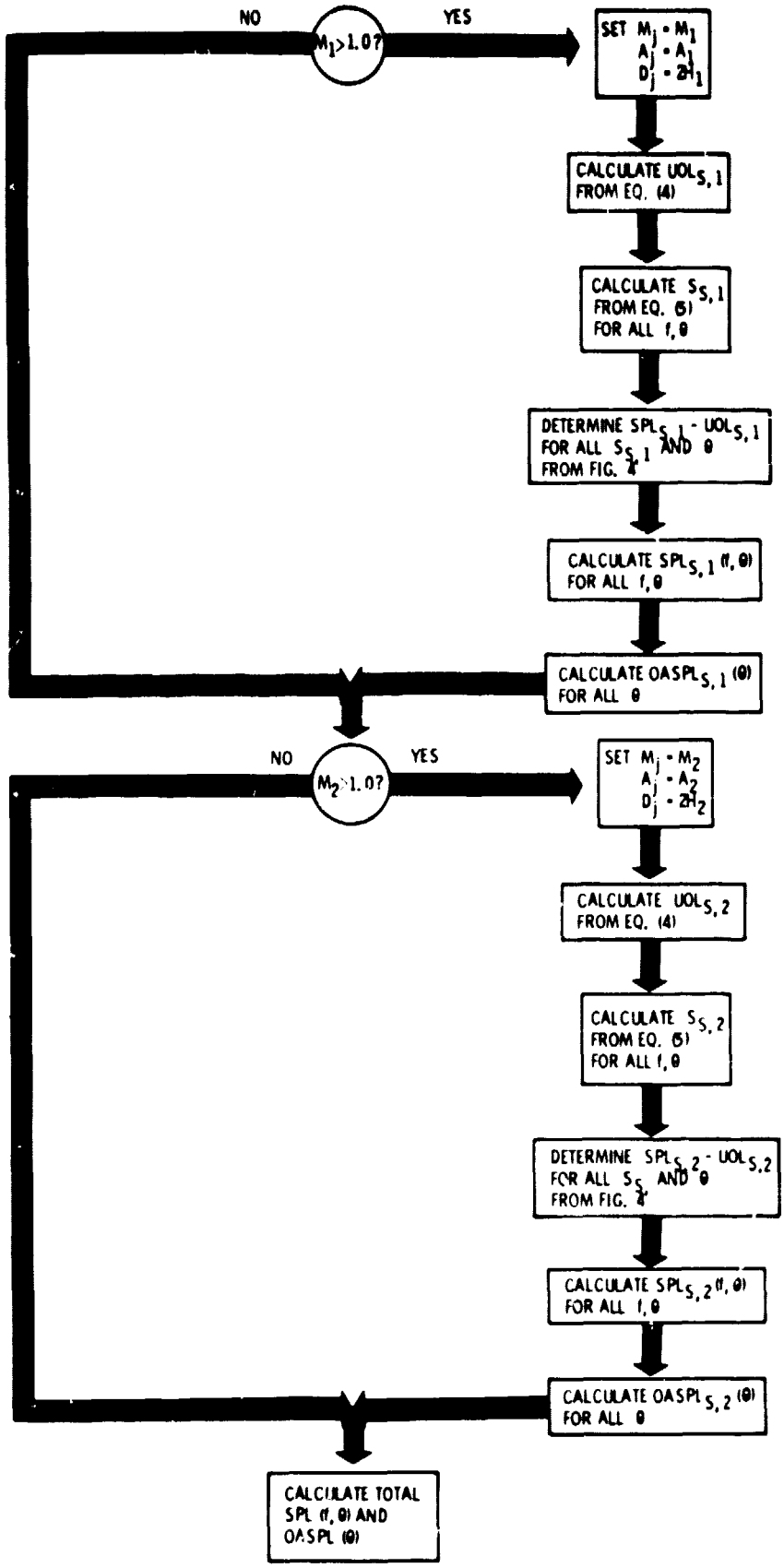

Figure 2. - Concluded

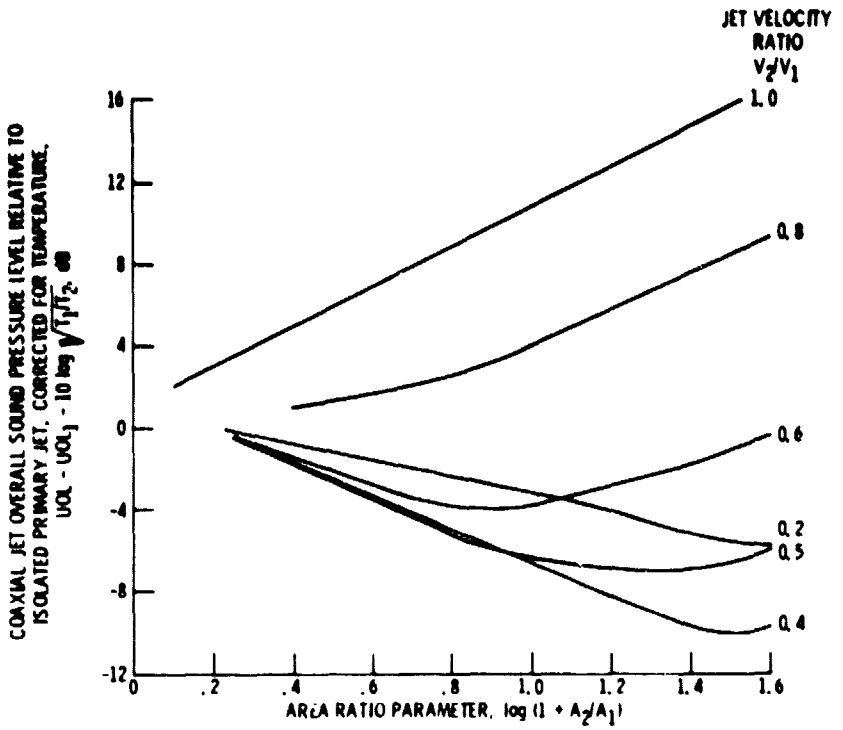

Figure 3. - Recommended prediction for coaxial jet OASPL relative to isolated primary jet, based on extension of the method of Olsen and Friedman (ref. 7), equation (1).

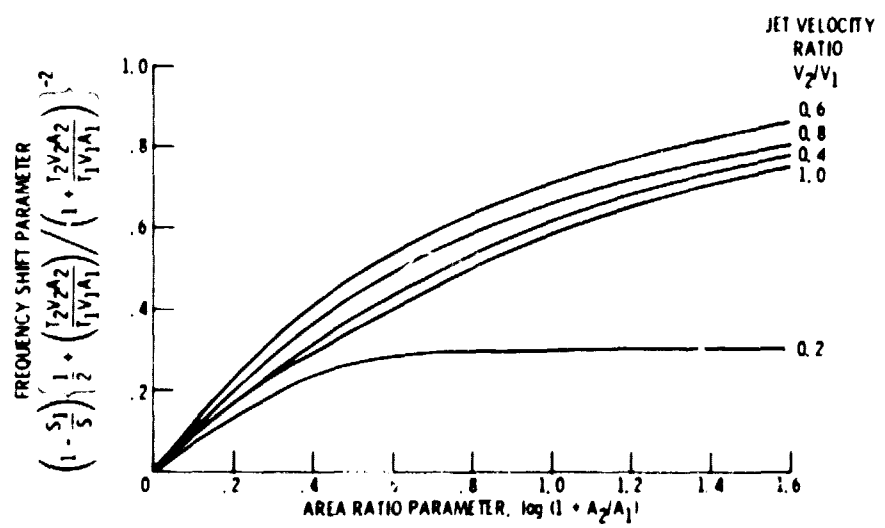

Figure 4. - Recommended frequency shift parameter for coaxial jets with respect to isolated primary jet, based on extension of the method of Olsen and Friedman (ref. 7).

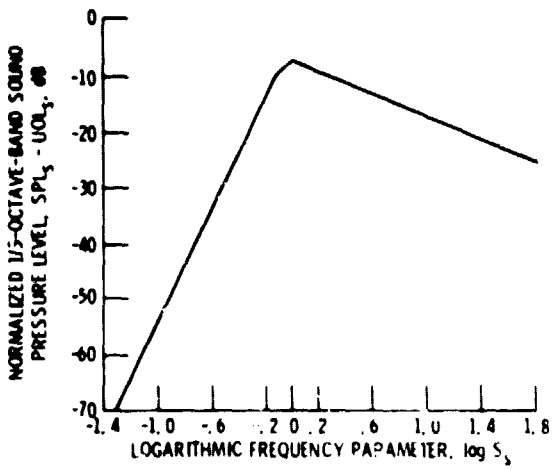

Figure 5. - Recommended 1/3-octave band spectrum for shock noise (ref. 4).

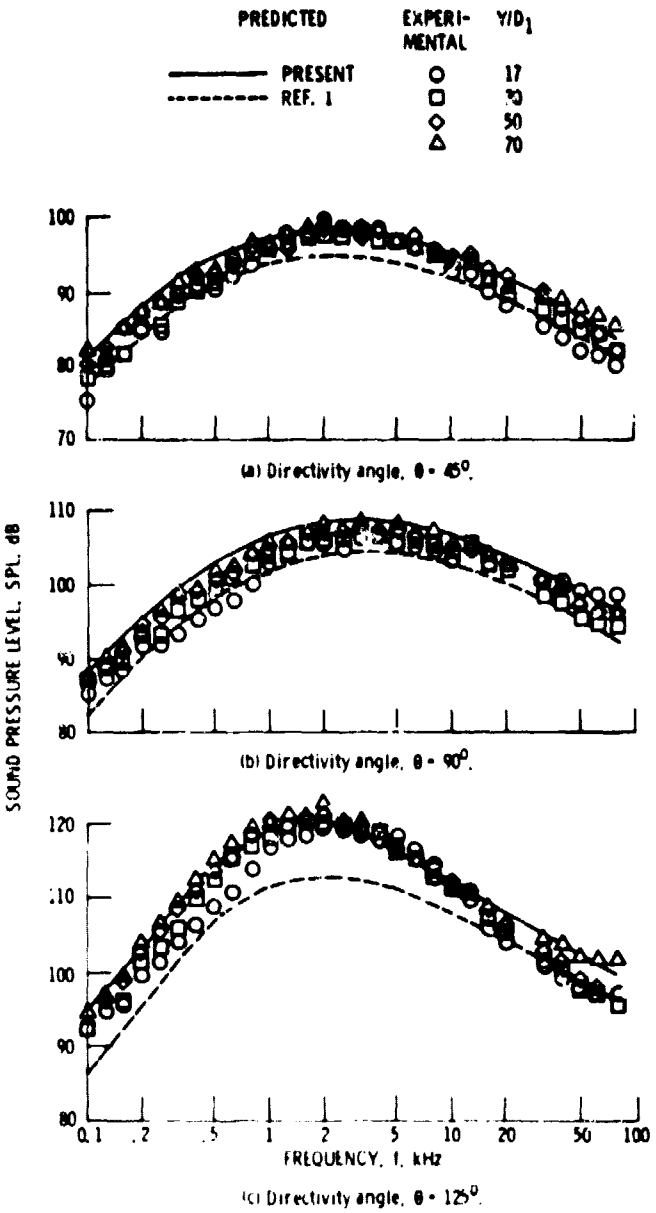

Figure 6. - Comparison of prediction with lossless free-field experimental subsonic spectra scaled to a 3.0-m sideline for 1.9-area-ratio coplanar coaxial nozzle with 10-cm diameter primary nozzle. Primary velocity, V_1 = 590 m/sec, and temperature, T_1 = 1132K; secondary velocity, V_2 = 216 m/sec, and temperature, T_2 = 248K.

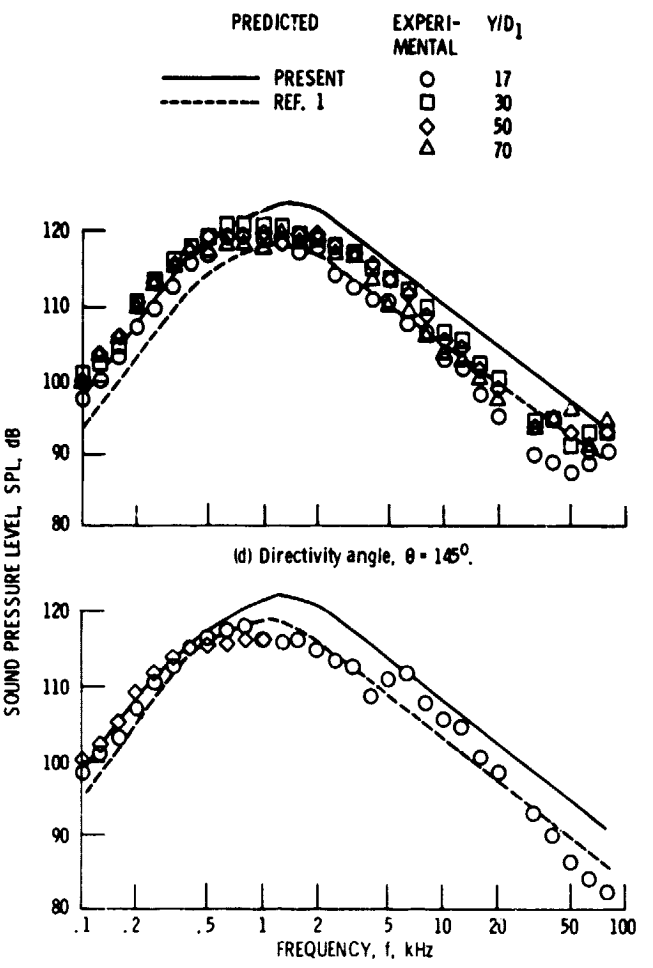

(d) Directivity angle, $\theta = 145^0$.

(e) Directivity angle, $\theta = 150^0$.

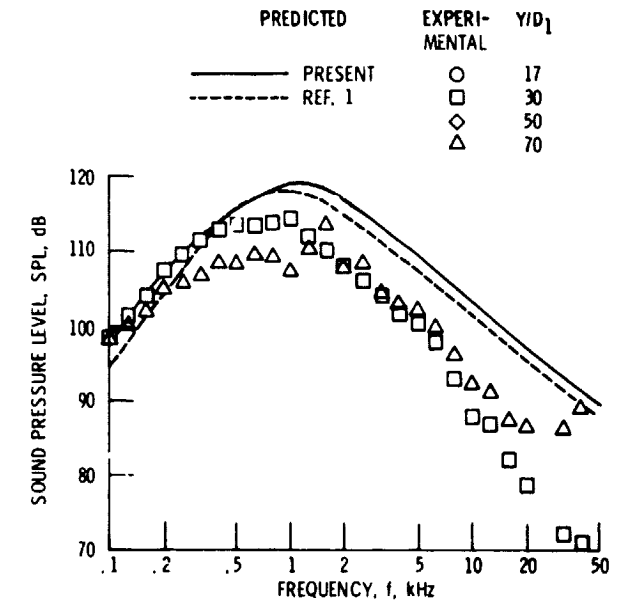

(f) Directivity angle, $\theta = 155^0$.

Figure 6. - Concluded.

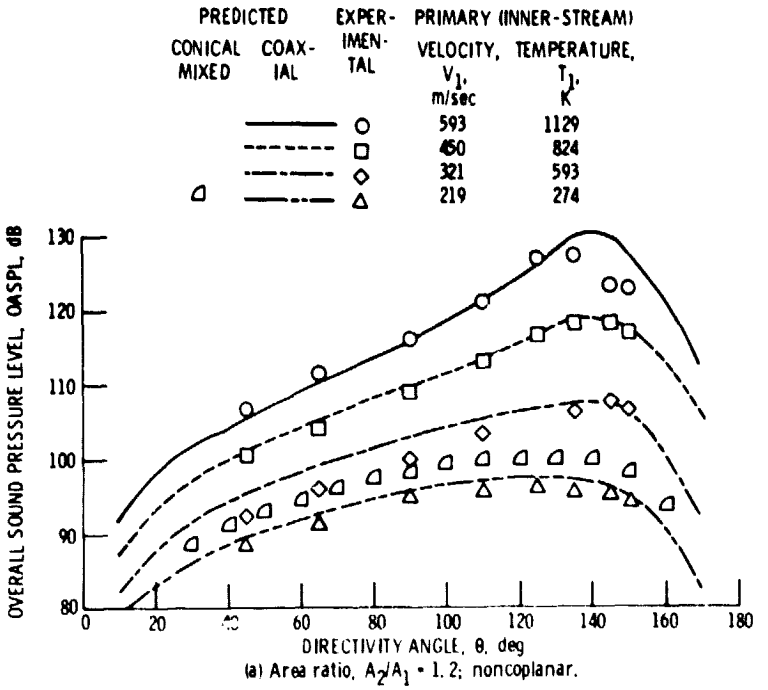

(a) Area ratio, $A_2/A_1 = 1.2$; noncoplanar.

Figure 7. - Comparison of predicted and experimental effect of primary conditions on lossless free-field OASPL directivity on 5.0-m sideline. Secondary velocity, $V_2 \approx 215$ m/sec, and temperature, $T_2 \approx 279$K.

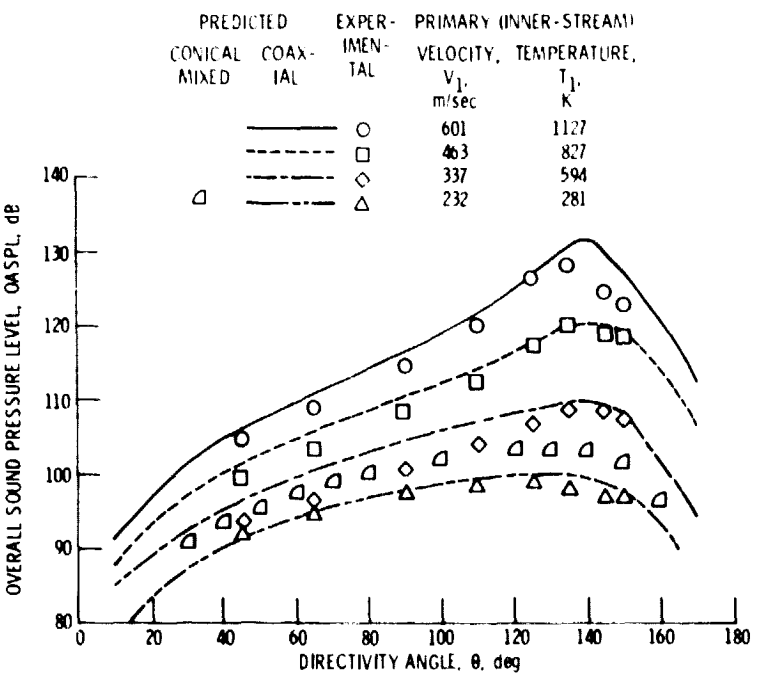

(b) Area ratio, $A_2/A_1 = 1.4$; coplanar.

Figure 7. - Continued.

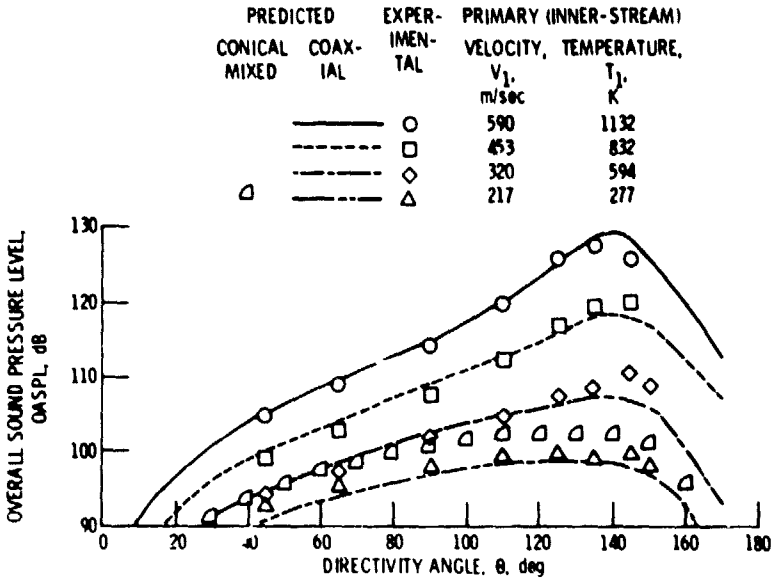

(c) Area ratio, 1.9; coplanar.

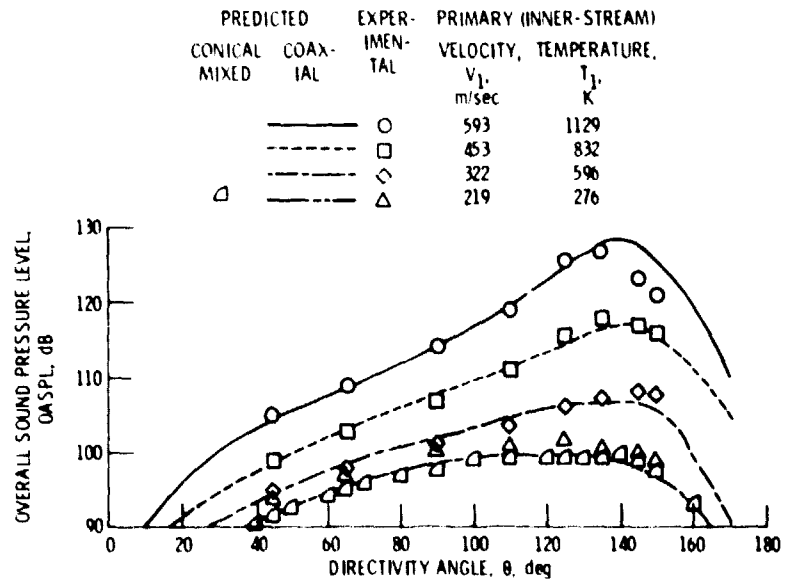

(d) Area ratio, 3.2, coplanar.

Figure 7. - Concluded.

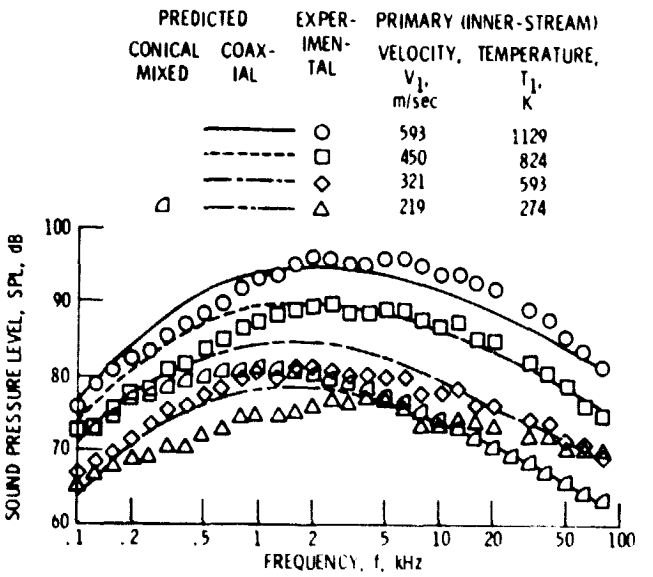

(a) Directivity angle, $\theta = 45^0$.

Figure 8. - Comparison of predicted and experimental effect of primary velocity and temperature on lossless free-field subsonic spectra at a 5.0-m sideline. 1.2-Area-ratio coaxial noncoplanar nozzle; primary nozzle diameter, $D_1 = 10.0$ cm; secondary velocity, V_2 215 m/sec, and temperature, T_2 279 K.

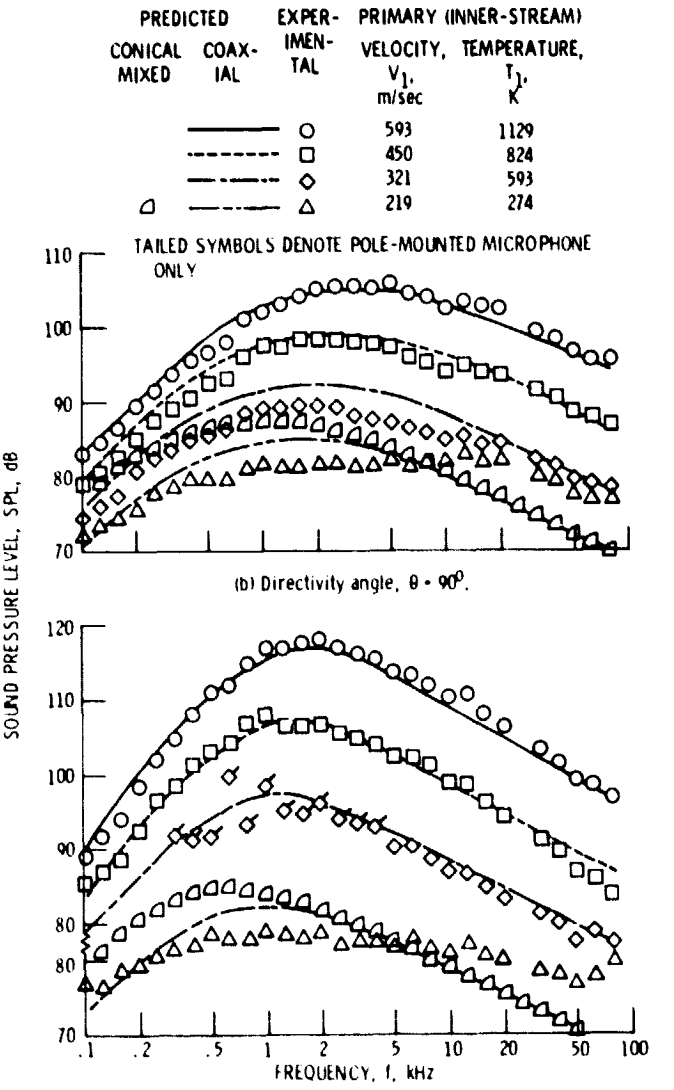

(b) Directivity angle, $\theta = 90^0$.

(c) Directivity angle, $\theta = 125^0$.

Figure 8. - Continued.

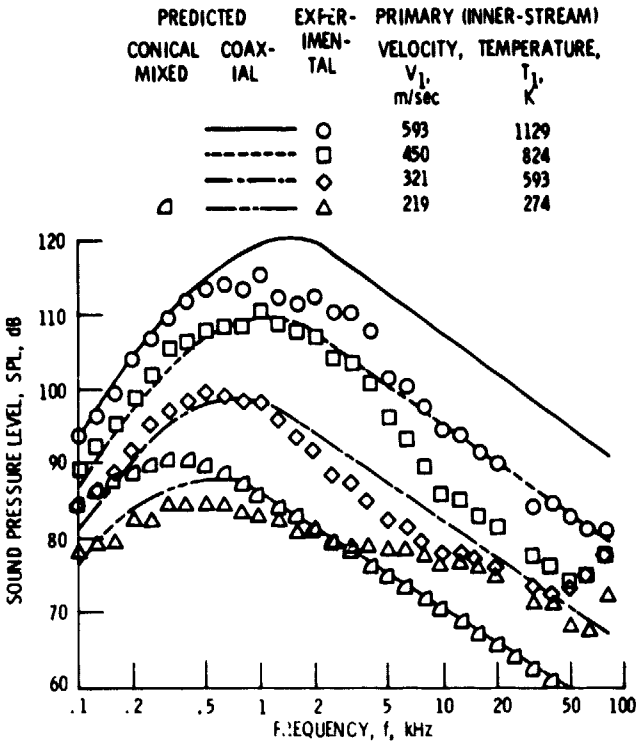

(d) Directivity angle, $\theta = 145^{\circ}$.

Figure 8. - Concluded.

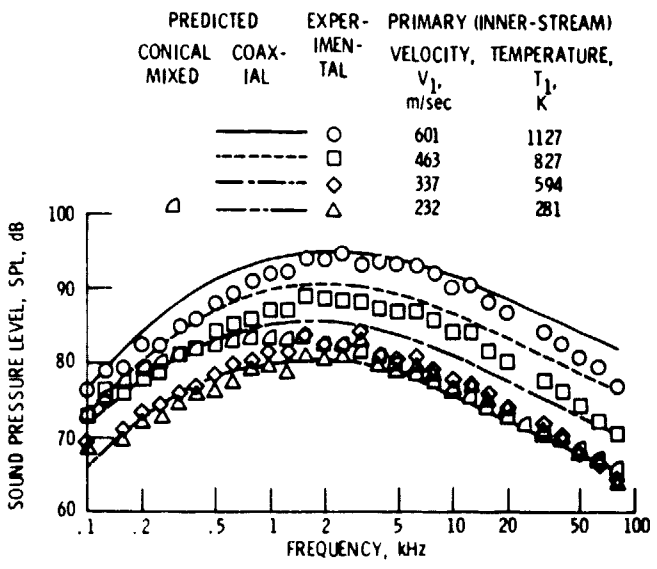

(a) Directivity angle, $\theta = 45^{\circ}$.

Figure 9. - Comparison of predicted and experimental effect of primary velocity and temperature on lossless free-field subsonic spectra at 5.0-m sideline. 1.4-Area-ratio coaxial coplanar nozzle; primary nozzle diameter, 10.0 cm; secondary velocity, $V_2 \approx 230$ m/sec, and temperature, $T_2 \approx 286$ K.

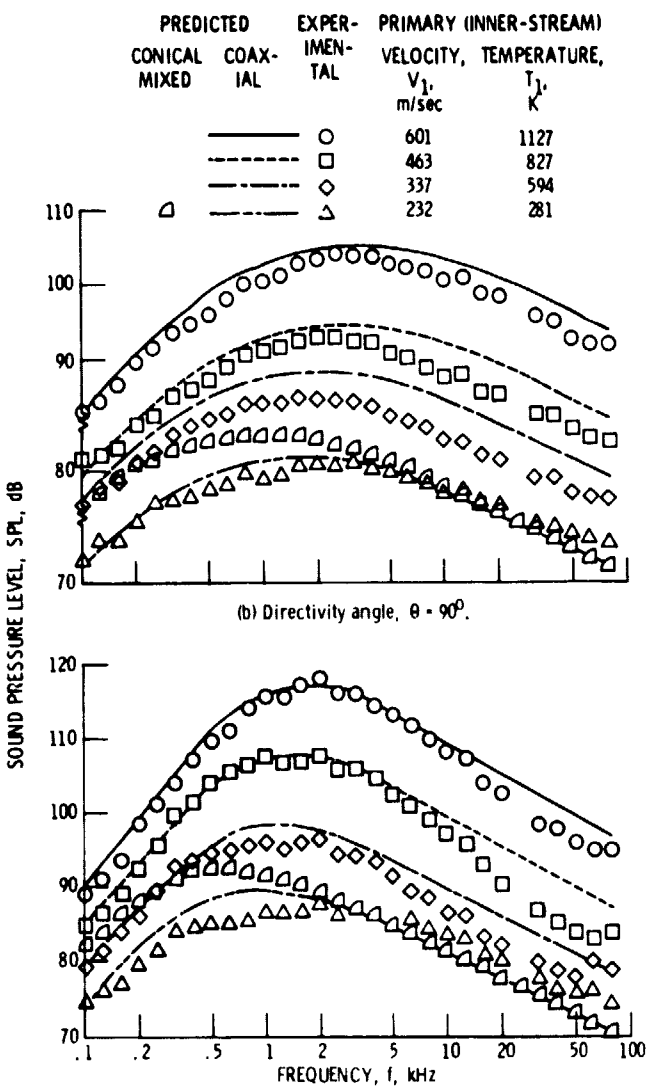

(b) Directivity angle, $\theta = 90^0$.

(c) Directivity angle, $\theta = 125^0$.

Figure 9. - Continued.

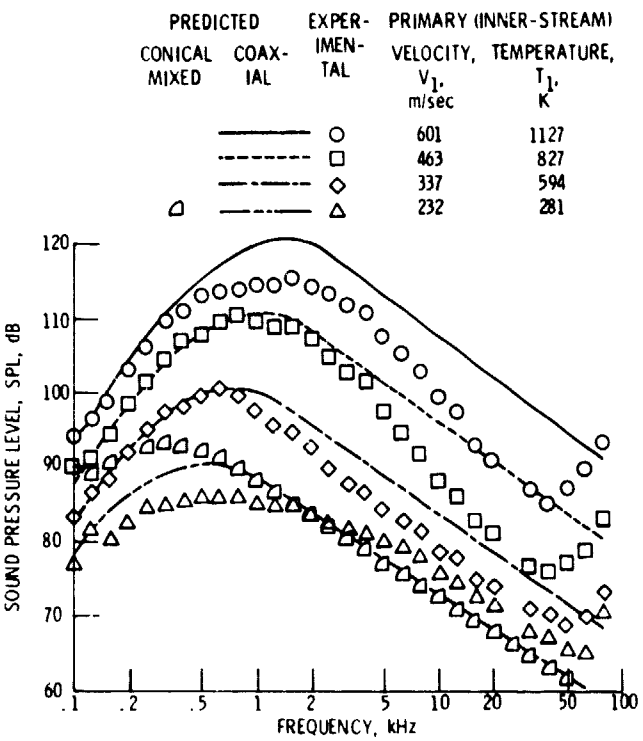

(d) Directivity angle, $\theta = 145^0$.

Figure 9. - Concluded.

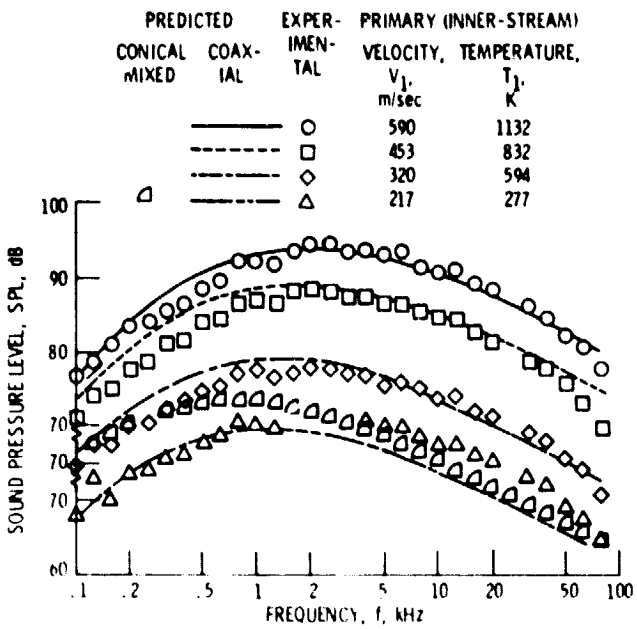

(a) Directivity angle, $\theta = 45^{\circ}$.

Figure 10. - Comparison of predicted and experimental effect of primary velocity and temperature on lossless free-field subsonic spectra on 5.0-m sideline. 1.9 Area-ratio coaxial coplanar nozzle, primary nozzle diameter, 10.0-cm, secondary velocity, V_2 = 217 m/sec, and temperature, T_2 = 277 K.

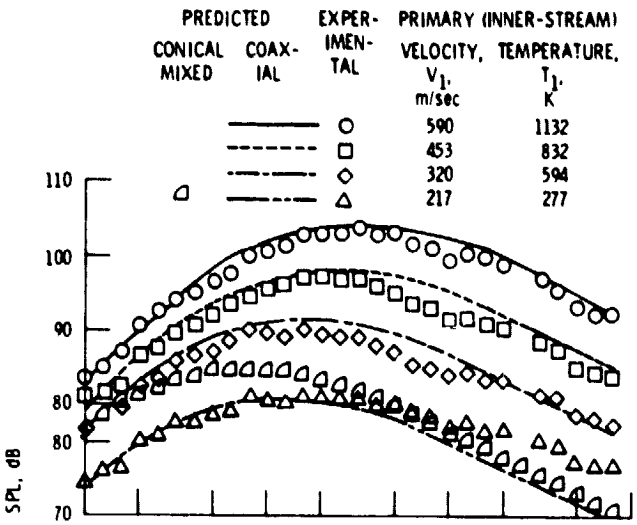

(b) Directivity angle, $\theta = 90^{\circ}$.

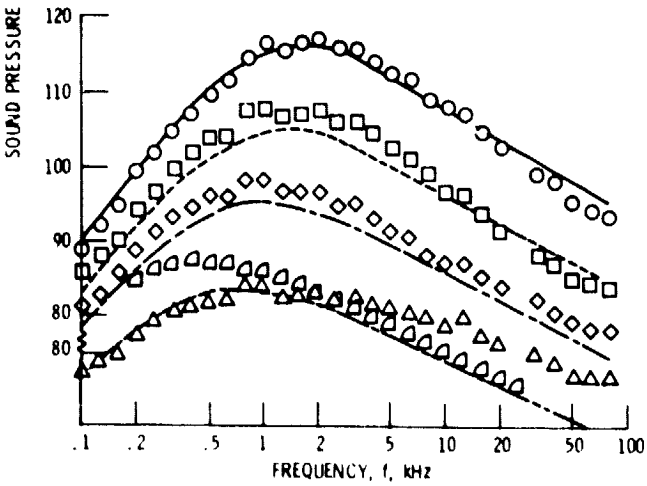

(c) Directivity angle, $\theta = 125^{\circ}$.

Figure 10. - Continued.

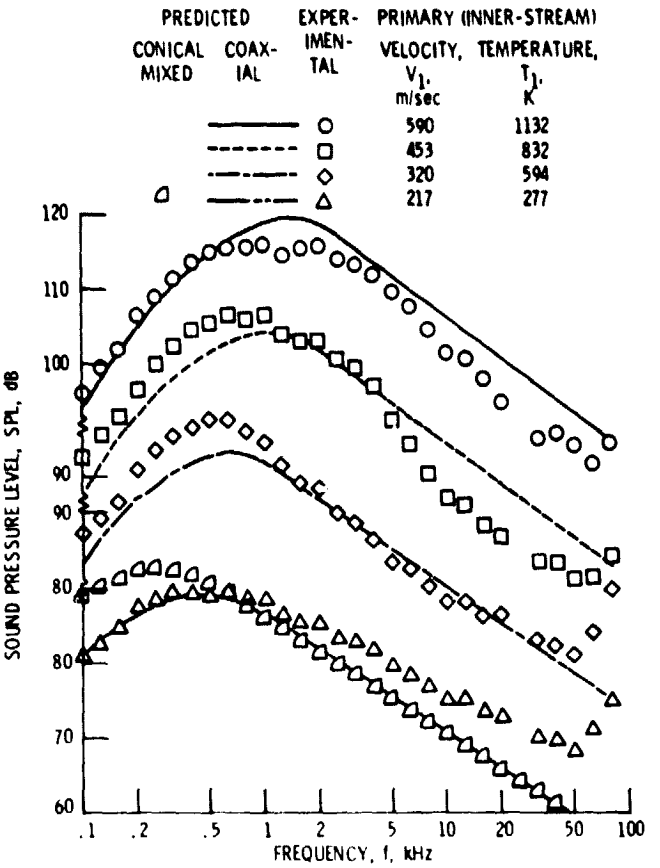

(d) Directivity angle, $\theta = 145^0$.

Figure 10. - Concluded.

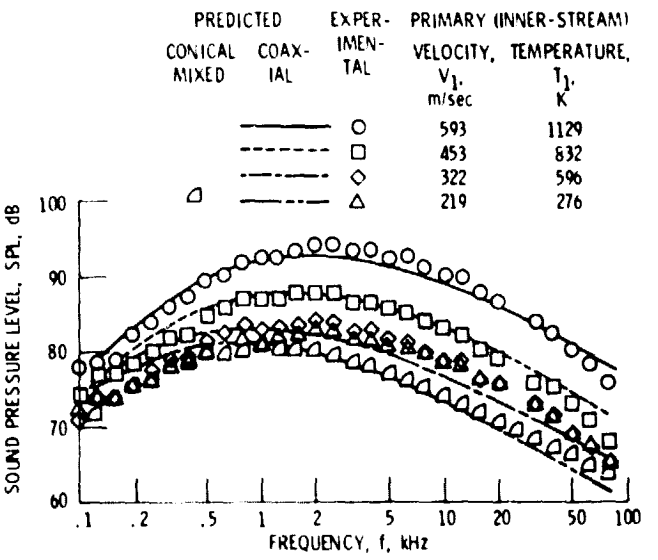

(a) Directivity angle, $\theta = 45^0$.

Figure 11. - Comparison of predicted and experimental effect of primary velocity and temperature on lossless free-field subsonic spectra at 5.0-m sideline. 3.2-Area-ratio coaxial coplanar nozzle, primary nozzle diameter, 10 cm, secondary velocity V_2 = 216 m/sec, and temperature, T_2 = 280 K.

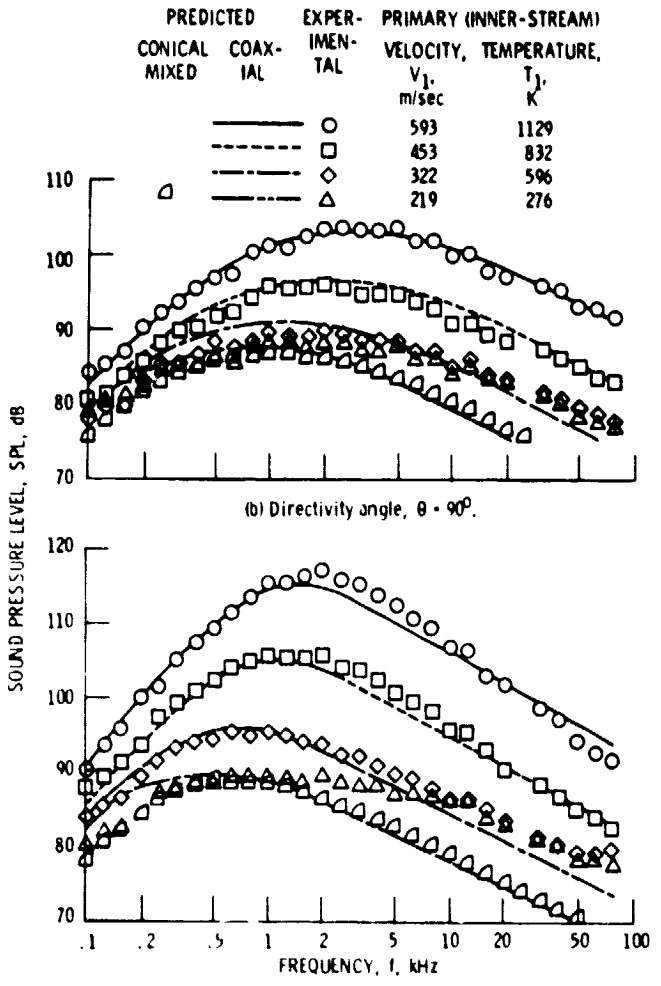

(b) Directivity angle, $\theta = 90^0$.

(c) Directivity angle, $\theta = 125^0$.

Figure 11. - Continued.

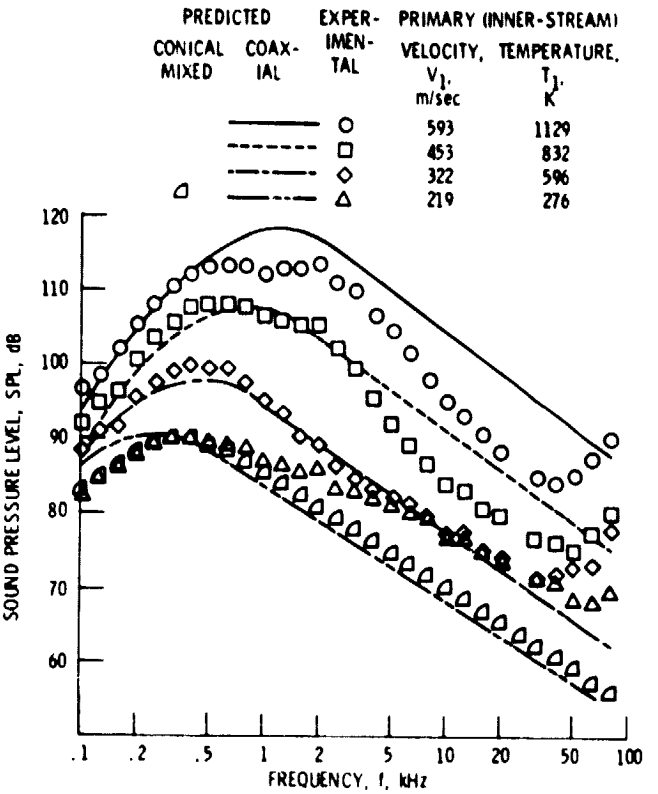

(d) Directivity angle, $\theta = 145^0$.

Figure 11. - Concluded.

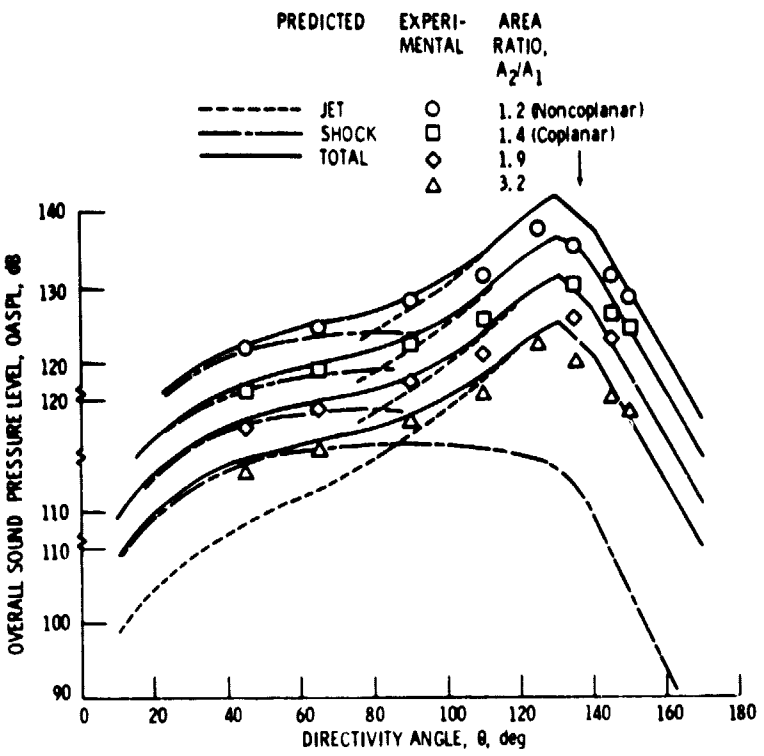

(a) High primary Mach no., $M_1 \approx 1.38$; high primary velocity, $V_1 \approx 790$ m/sec ($T_1 \approx 1130$ K).

Figure 12. - Comparison of predicted and experimental effect of area ratio on supersonic jet mixing and shock noise lossless free-field OASPL directivity on 5.0-m sideline. Primary nozzle diameter, 10.0 cm; subsonic secondary velocity, $V_2 \approx 216$ m/sec, and temperature, $T_2 \approx 278$ K (data of ref. 11).

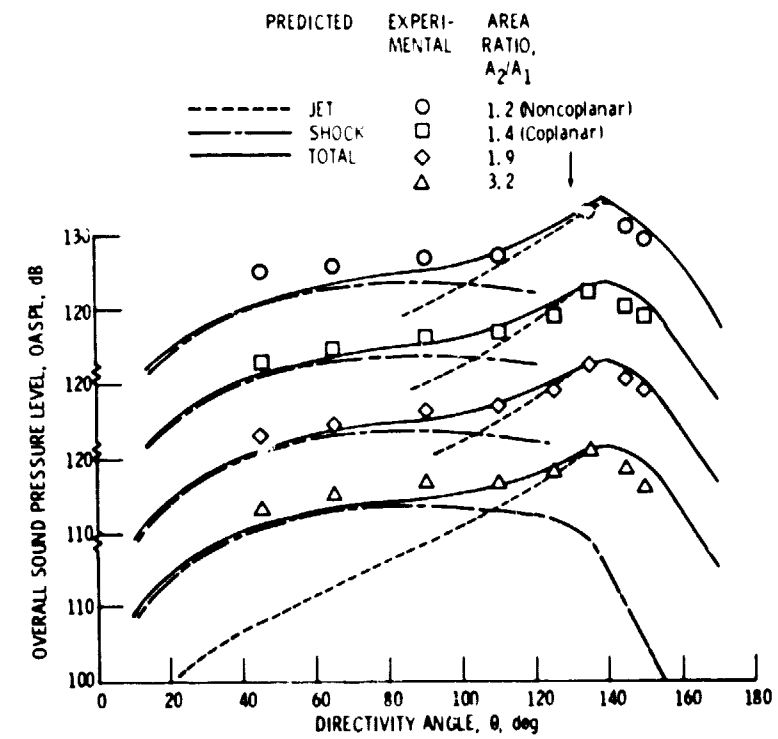

(b) High primary Mach no., $M_1 \approx 1.38$; moderate primary velocity, $V_1 \approx 570$ m/sec ($T_1 \approx 600$ K).

Figure 12. - Continued.

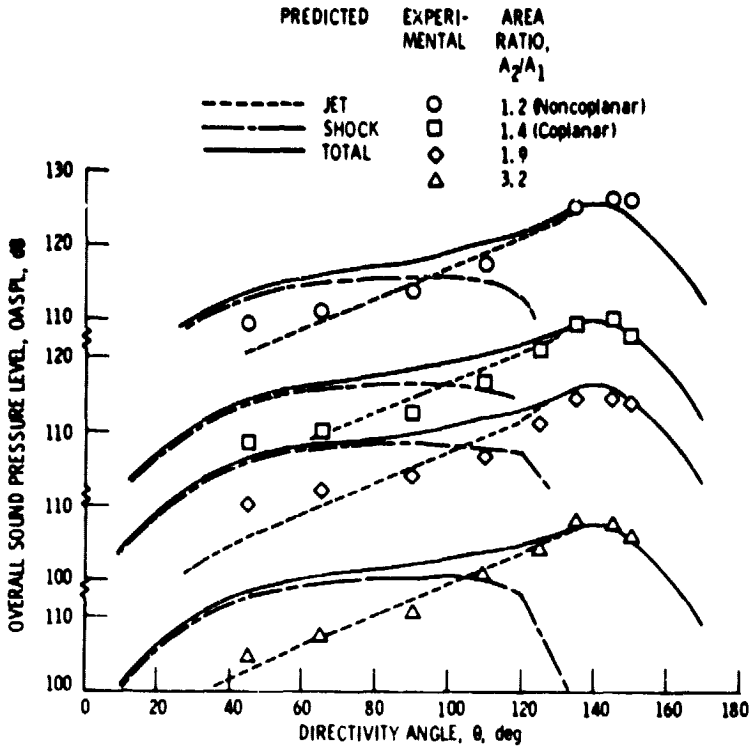

(c) Low primary Mach no., $M_1 = 1.13$; low primary velocity, $V_1 = 490$ m/sec ($T_1 = 590$ K).

Figure 12. - Concluded.

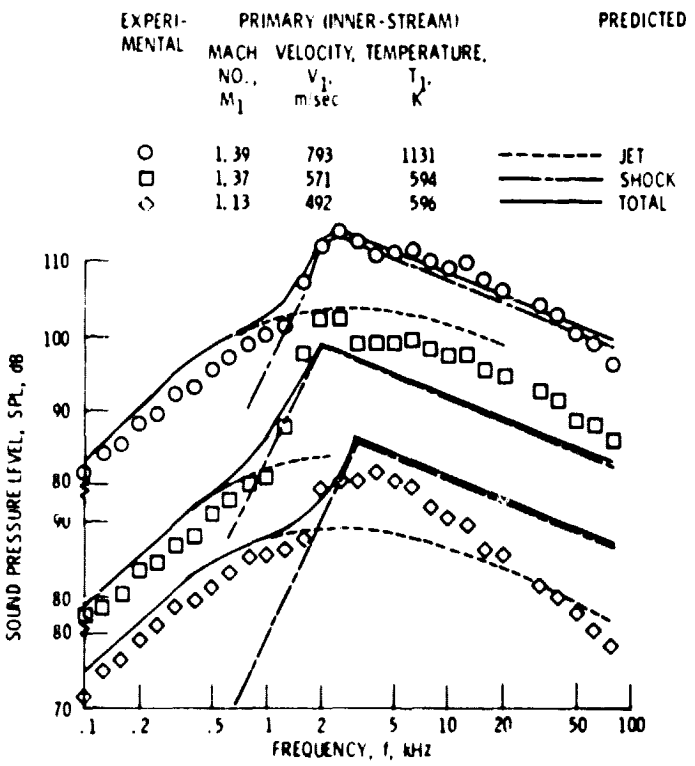

(a) Directivity angle, $\theta = 45^\circ$.

Figure 13. - Comparison of predicted and experimental effect of supersonic primary conditions on lossless free-field spectra at 5.0-m sideline. 1.2-Area-ratio noncoplanar coaxial nozzle, primary diameter 10 cm, secondary velocity, $V_2 = 215$ m/sec, and temperature, $T_2 = 279$ K.

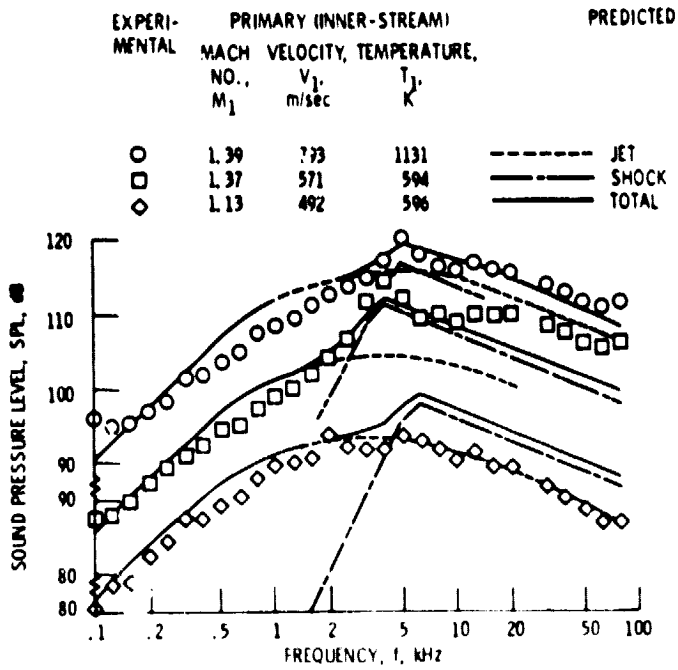

(b) Directivity angle, $\theta = 90^0$.

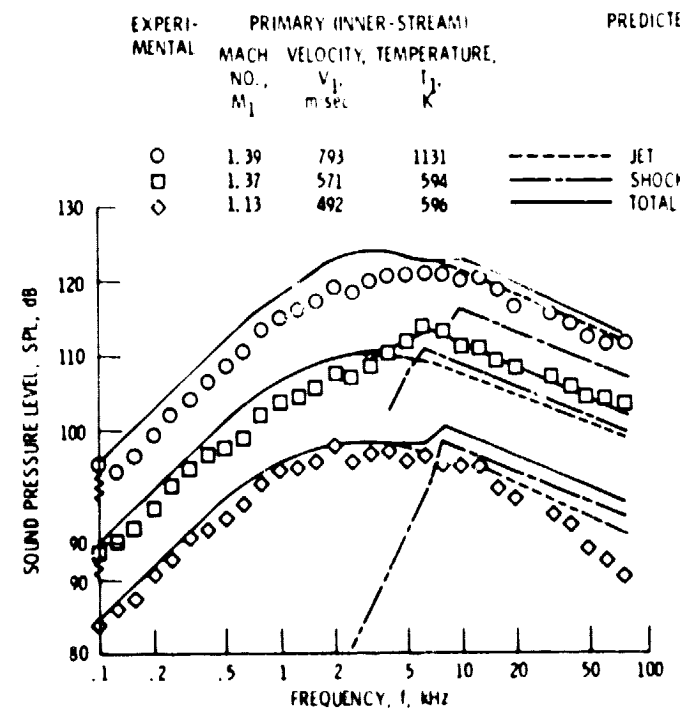

(c) Directivity angle, $\theta = 110^0$.

Figure 13. - Continued.

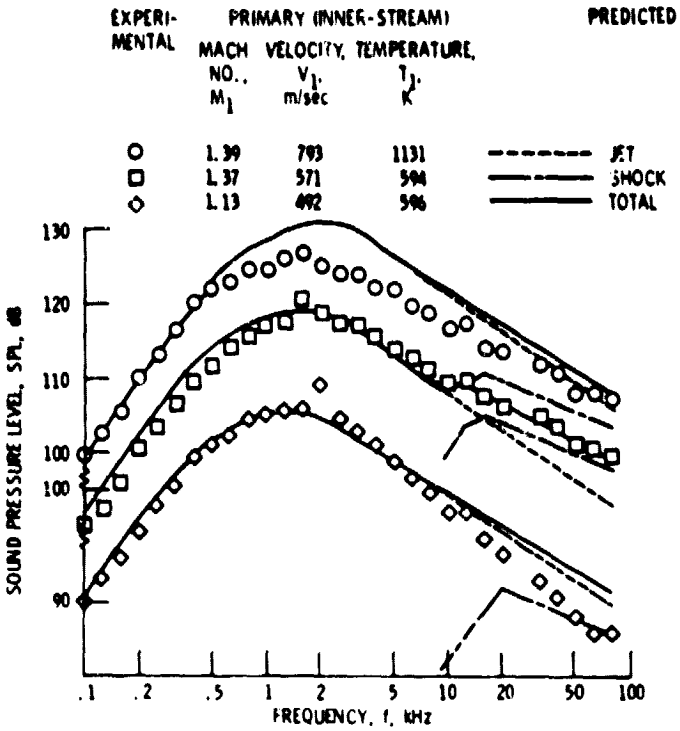

(d) Directivity angle, $\theta = 135^{\circ}$.

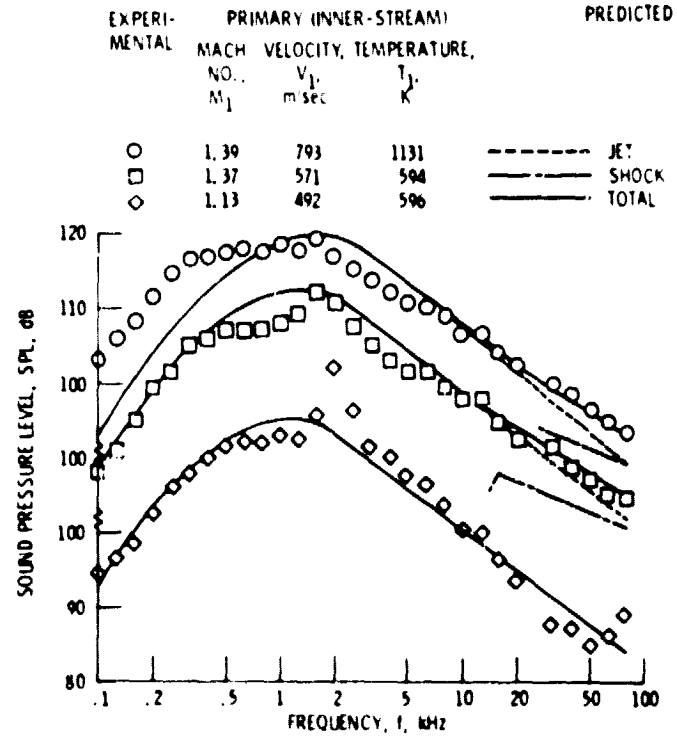

(e) Directivity angle, $\theta = 150^{\circ}$.

Figure 13. - Concluded.

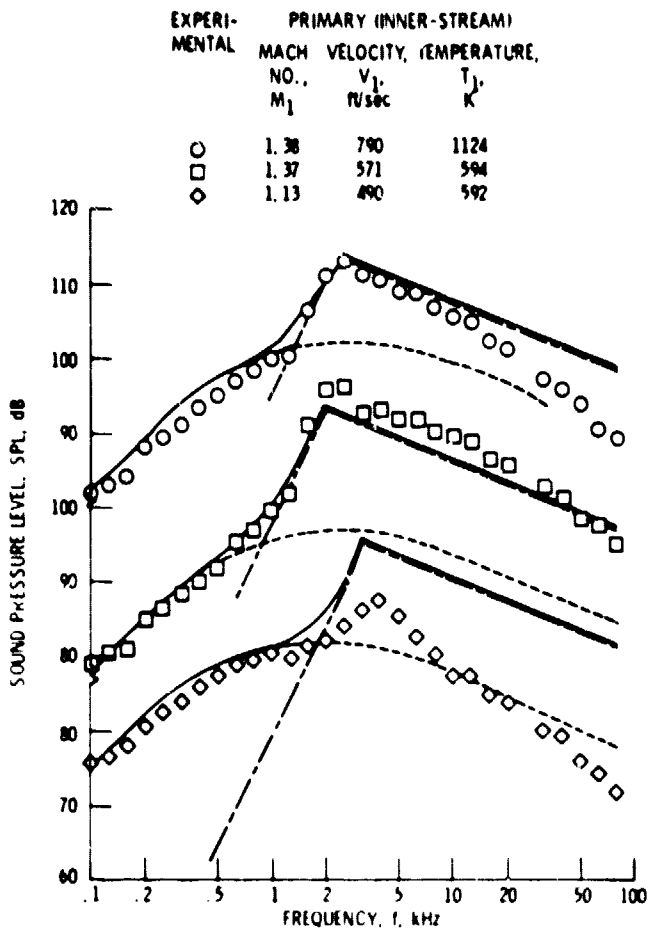

(a) Directivity angle, $\theta = 45^0$.

Figure 14. - Comparison of predicted and experimental effect of supersonic primary conditions on lossless free-field spectra at 5.0-m sideline. 3.2-area-ratio coplanar coaxial nozzle, primary diameter, 10-cm; secondary velocity, V_2 216 m/sec, and temperature, $T_2 = 280K$.

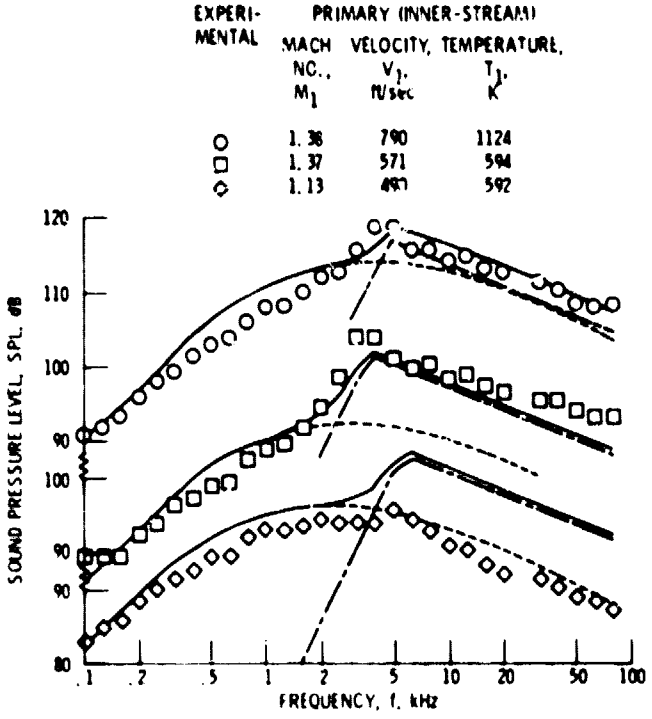

(b) Directivity angle, $\theta = 90^0$.

Figure 14. - Continued.

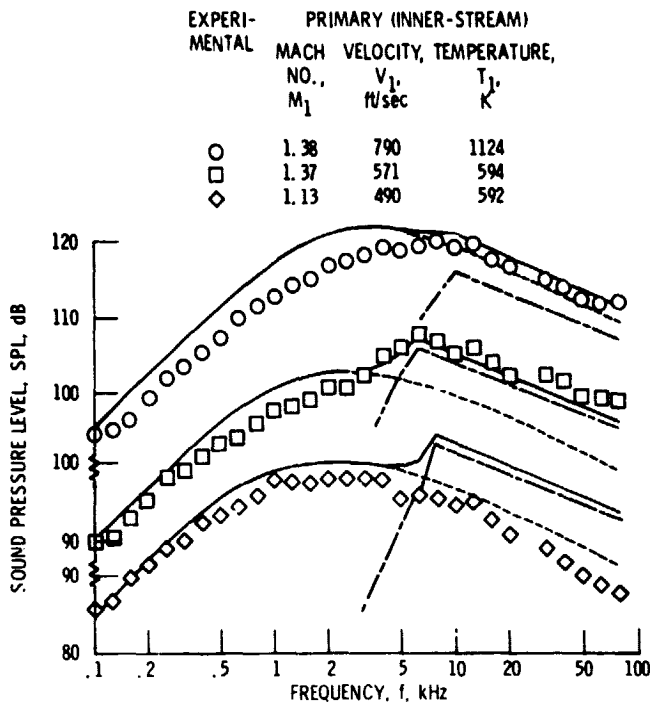

(c) Directivity angle, $\theta = 110^0$.

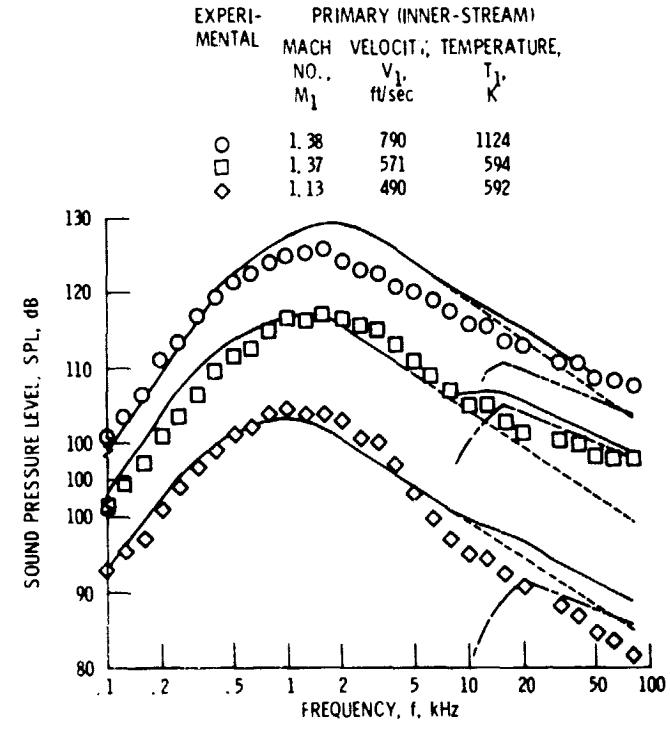

(d) Directivity angle, $\theta = 135^0$.

Figure 14. - Continued.

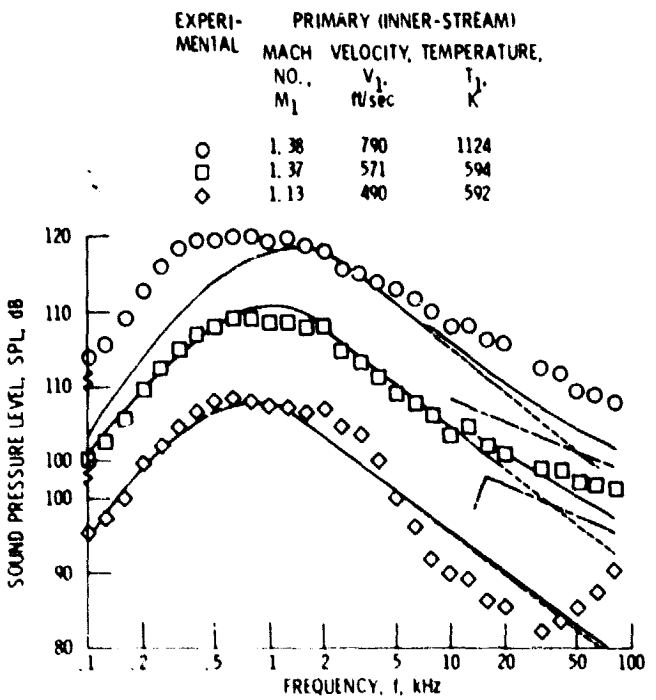

(e) Directivity angle, $\theta = 150^{\circ}$.

Figure 14. - Concluded.

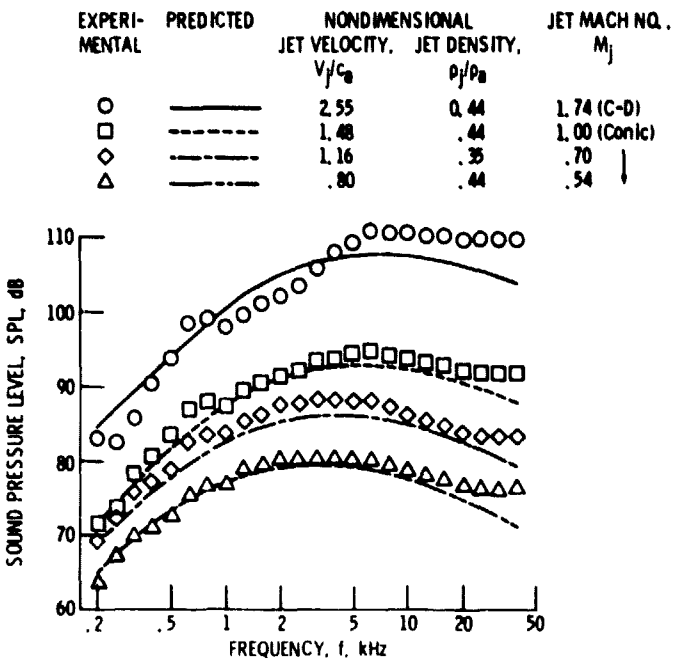

(a) Directivity angle, $\theta = 57^0$.

Figure A1. - Comparison of predicted and experimental effect of single-stream jet conditions on lossless free-field shock-free spectra on a 3.66-m arc. Experimental data of Tanna, et al. (ref. 13) for 5.08-cm diameter conical and circular convergent-divergent nozzles.

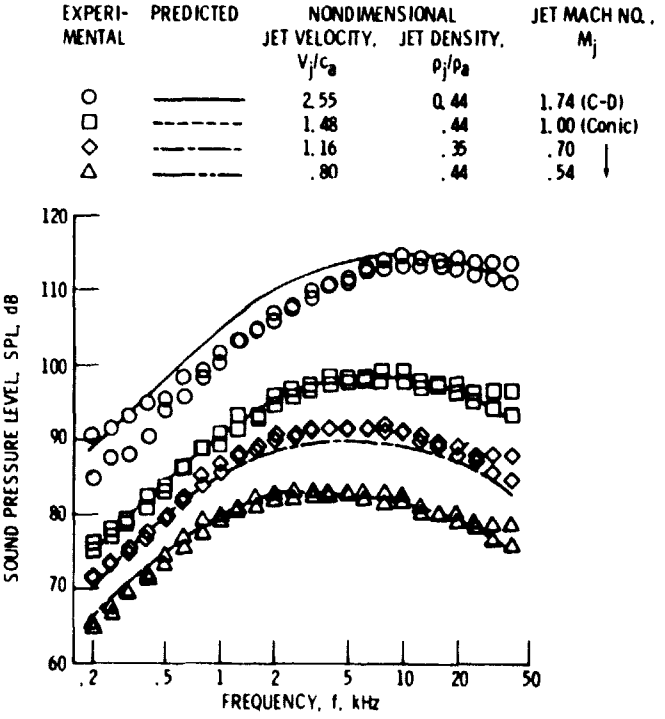

(b) Directivity angle, $\theta = 86^0$.

Figure A1. - Continued.

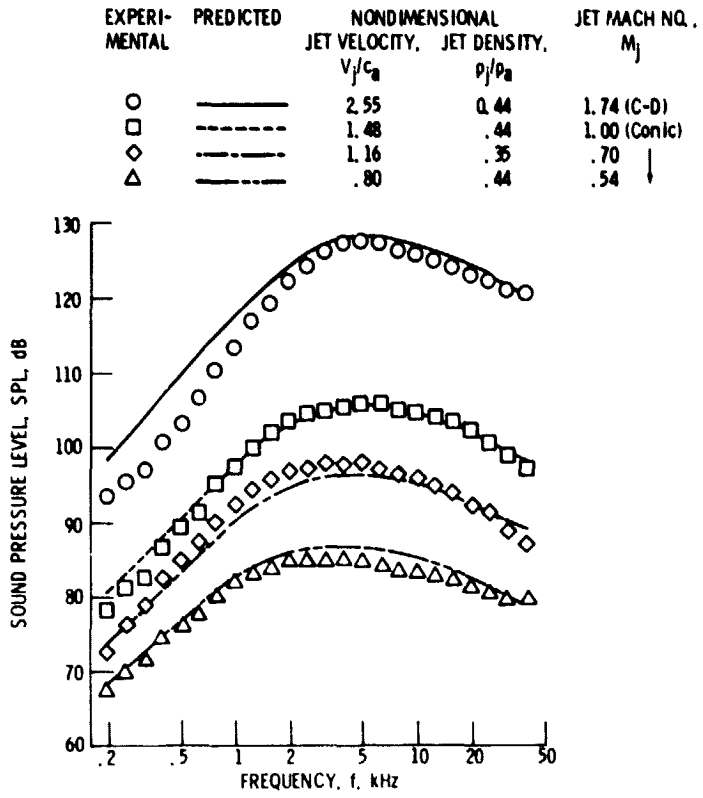

(c) Directivity angle, $\theta = 116^0$.

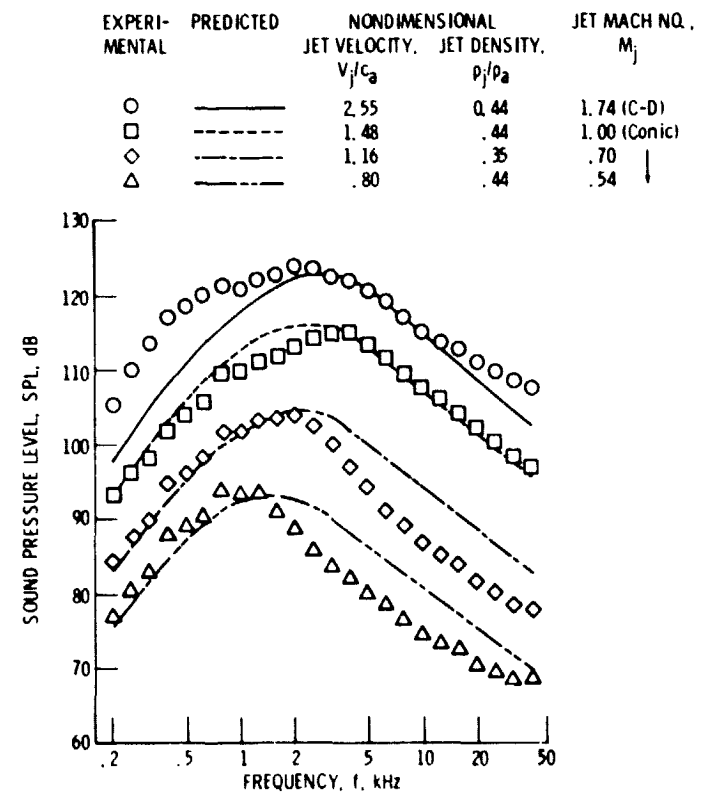

(d) Directivity angle, $\theta = 155^0$.

Figure A1. - Concluded.

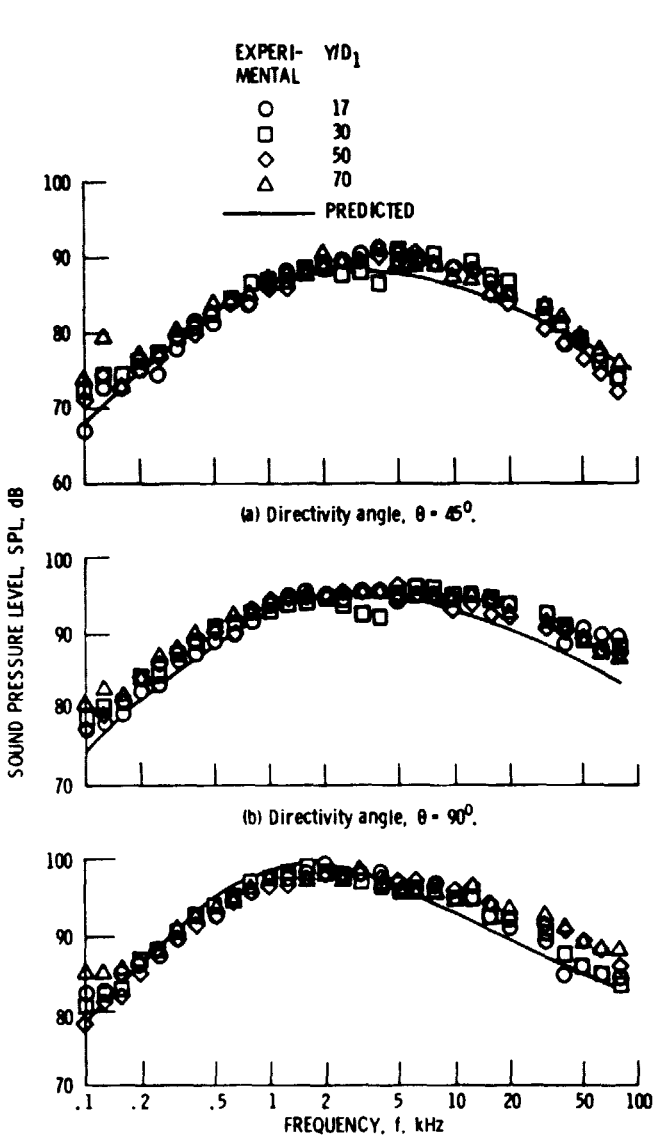

(a) Directivity angle, $\theta = 45^0$.

(b) Directivity angle, $\theta = 90^0$.

(c) Directivity angle, $\theta = 125^0$.

Figure A2. - Comparison of prediction with lossless free-field experimental data scaled to 3.0-m (9.8-ft) sideline for 3.2-area-ratio coplanar coaxial nozzle. Inner-stream velocity, $V_1 \approx 295$ m/sec (967 ft/sec), and temperature $T_1 \approx 287$ K (517 ^{0}R); outer-stream (no flow).

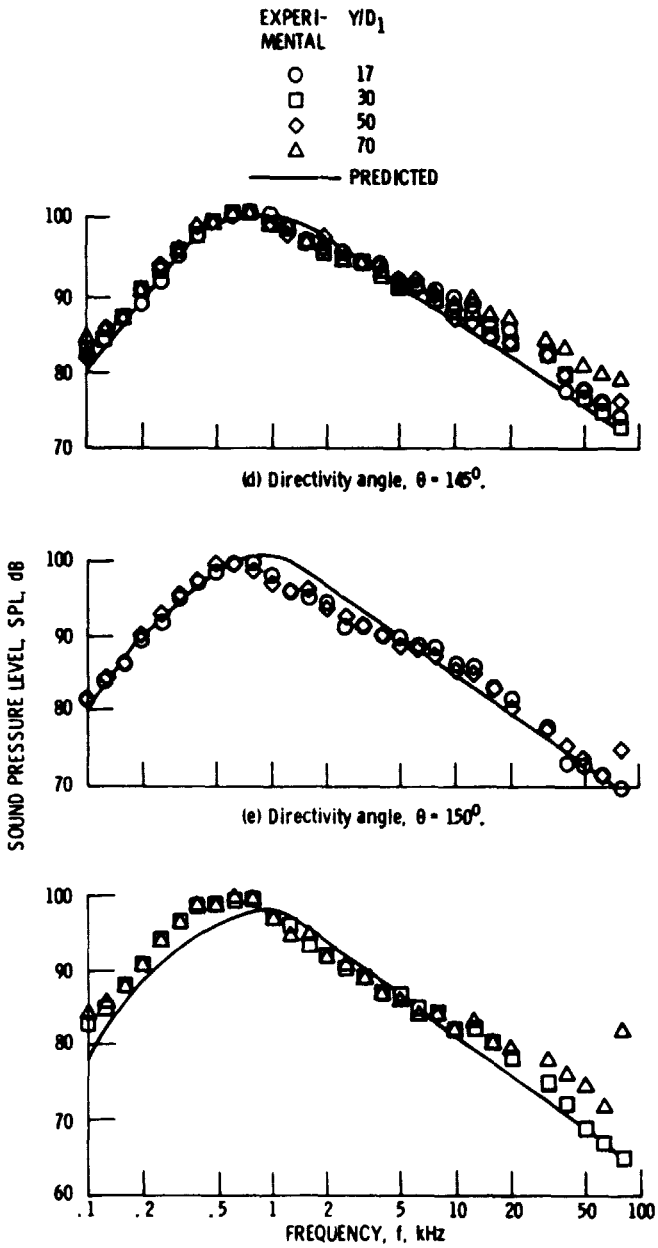

(d) Directivity angle, $\theta = 145^0$.

(e) Directivity angle, $\theta = 150^0$.

(f) Directivity angle, $\theta = 155^0$.

Figure A2. - Concluded.